LETTERS
https://doi.org/10.1038/s41562-018-0324-5
nature human behaviour

Multiple motor memories are learned to control different points on a tool

James B. Heald[1*], James N. Ingram[1], J. Randall Flanagan[2] and Daniel M. Wolpert[1]

Skilful object manipulation requires learning the dynamics of objects, linking applied force to motion[1,2]. This involves the formation of a motor memory[3,4], which has been assumed to be associated with the object, independent of the point on the object that one chooses to control. Importantly, in manipulation tasks, different control points on an object, such as the rim of a cup when drinking or its base when setting it down, can be associated with distinct dynamics. Here, we show that opposing dynamic perturbations, which interfere when controlling a single location on an object, can be learned when each is associated with a separate control point. This demonstrates that motor memory formation is linked to control points on the object, rather than the object per se. We also show that the motor system only generates separate memories for different control points if they are linked to different dynamics, allowing efficient use of motor memory. To account for these results, we develop a normative switching state-space model of motor learning, in which the association between cues (control points) and contexts (dynamics) is learned rather than fixed. Our findings uncover an important mechanism through which the motor system generates flexible and dexterous behaviour.

Understanding how humans learn to use tools is a central challenge in neuroscience[5]. Tool use requires knowledge of the dynamics of objects (relating applied force to motion), which depends on both the physical properties of objects (for example, mass, mass distribution and friction) and how objects are used to interact with the environment (for example, for transport or percussion). Numerous paradigms have been developed to explore how humans learn the dynamics of objects. In conventional object-manipulation tasks, participants grasp and lift physical objects with familiar dynamics[3,6,7]. When lifting an object for the first time, visual cues about size and surface material strongly influence lift forces[8–10]. However, after several lifts, participants learn the dynamics of the object, as demonstrated by adaptation of grip and lift forces measured at the fingertips before object lift off[1,11]. If the dynamics of the object is simple, learning can occur in a single trial[8]. However, even for objects with simple dynamics, interference can be seen when alternately lifting the same object and grasping it at different locations[12,13].

Robotic manipulanda offer an alternative testbed for object-manipulation studies[14]. These interfaces can simulate objects with unfamiliar dynamics[15–20] and provide an opportunity to manipulate the relationship between haptic and visual feedback[21,22]. In a typical adaptation experiment, participants grasp the handle of a robotic manipulandum and make reaching movements that are perturbed by the robot. For example, a perturbation that has been examined extensively is a viscous curl field that generates forces on the hand that act perpendicular to the velocity of the hand and proportional to its speed[15,23–25]. Over repeated movements, participants learn to generate the forces required to compensate for the perturbation, forming a motor memory of the grasped object[26,27]. However, the capacity to learn different dynamics in such paradigms appears to be surprisingly limited when the same movement is made (under veridical visual feedback) in force fields that act in opposite directions[28,29].

In the standard force-field adaptation paradigm, the 'object' being moved to a target is a small disc and the task involves controlling the centre of the disc. However, in natural object-manipulation tasks involving objects with more complex geometries, we can exert control over different locations, or 'control points', on the object. For example, when using a wide broom to sweep along a wall, we could control the edge of the broom that is nearest to the wall to make contact with the wall. Such contact will perturb the head of the broom, rotating it in opposite directions for walls on the left and right; that is, when controlling the left and right side of the broom. Similarly, when drinking from a wine glass, we can control the near rim as we lift the glass to our mouth and then control the base of the stem as we replace the glass. Numerous studies of object manipulation have examined how memories of object dynamics transfer across changes in grasp configurations[12,13,30–34]. However, none of these previous studies have explicitly manipulated the location of the control point independently of either the grasp location or the required movement of the object.

Here, we tested the hypothesis that the motor system can flexibly engage separate memories when controlling different points on a single object, allowing different dynamics to be learned and associated with these control points. Using a planar robotic interface and virtual-reality system, we linked the movement of a rectangular virtual object to the motion of the hand. The hand was clearly visible at all times and located at the centre of the object (Fig. 1). There were two control points, located on the left and right of the object, and two corresponding targets. The two control points were linked to opposing viscous curl fields. On each trial, the participant was required to generate a straight ahead hand movement to align either the left or right control point with its corresponding target. Thus, the required movement was the same for both control points.

We found that participants could learn opposing dynamics when it was linked to these different points. By testing generalization, we show that this learning is associated with control points, rather than hand or target locations. In addition, we show that the motor system only assigns distinct memories to control points if they are linked to different dynamics, allowing flexible and efficient use of motor memory. Finally, we show that our results are best accounted for by a normative switching state-space model (SSSM). Unlike standard state-space models (SSMs), the SSSM can learn the probability of cues (that is, control points) given the context (that is, force field)

[1]Computational and Biological Learning Laboratory, Department of Engineering, University of Cambridge, Cambridge, UK. [2]Center for Neuroscience Studies and Department of Psychology, Queen's University, Kingston, ON, Canada. *e-mail: jbh40@cam.ac.uk

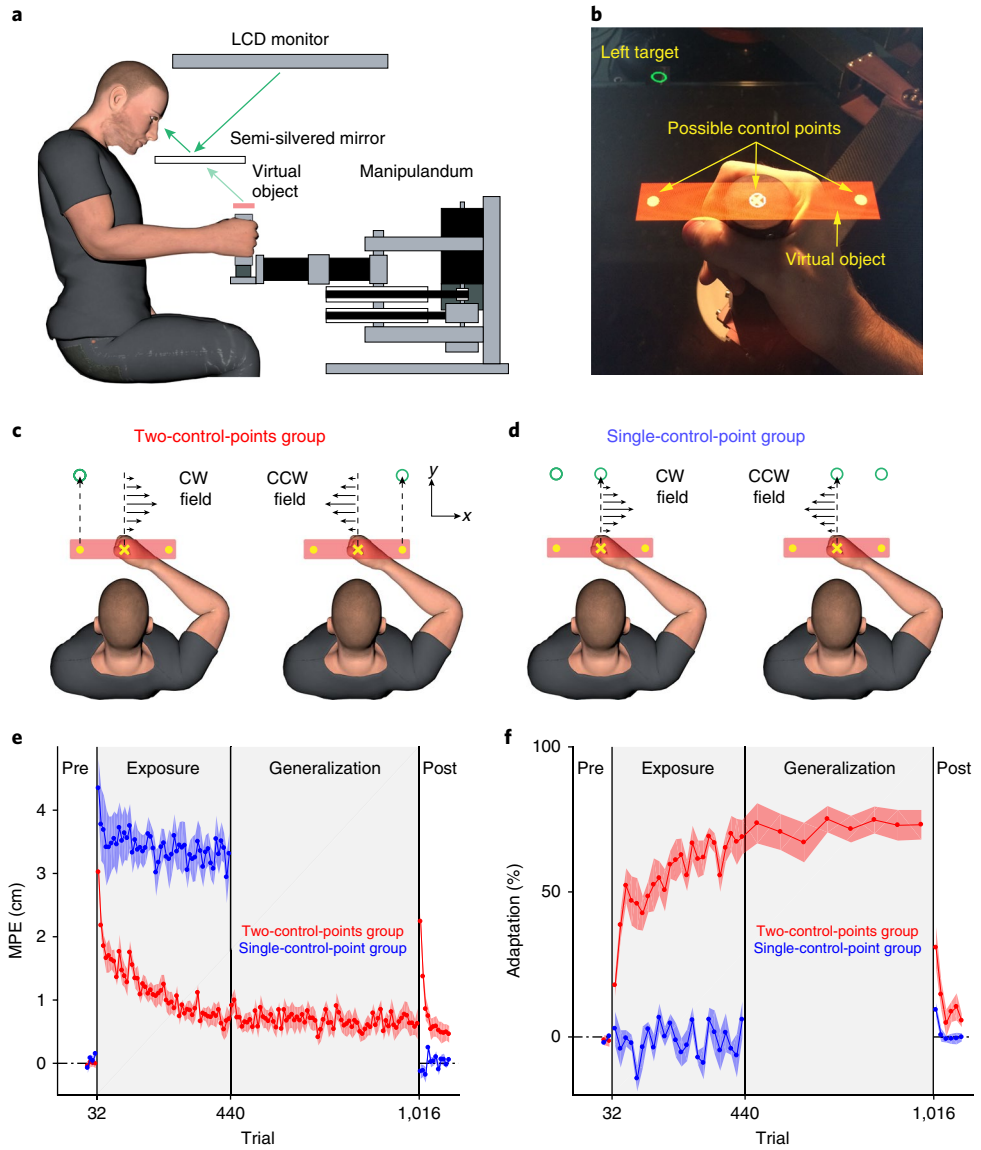

Fig. 1 | Separate motor memories are formed for different control points. Experimental paradigm and learning curves for experiment 1. **a**, Participants grasped the handle of a robotic manipulandum. A semi-silvered mirror allowed the participant to view their hand as well as a virtual object that was reflected from the monitor. LCD, liquid-crystal display. **b**, Photograph of the hand, virtual object and target as seen from the perspective of the participant. Depending on the experiment and trial type, one of three control points on the object had to be aligned with a target placed above it. **c**, Participants in the two-control-points group moved the left or right control point to its corresponding target. The direction of the force field applied to the hand was determined by the target/control point. **d**, Participants in the single-control-point group moved the central control point to a central target. The direction of the field applied to the hand was cued by which lateral 'target' was displayed. **e**, Kinematic error measured as the MPE (deviation from a straight line to the target) over the course of the experiment. Data were first averaged over blocks of eight exposure trials and then plotted as mean ± s.e.m. across participants. The grey background shows the period when the force field was turned on. **f**, Same as **e**, but for percentage adaptation measured on channel trials. The generalization phase was performed by the two-control-points group ($n = 10$), but omitted for the single-control-point group ($n = 8$).

and infer the state for each context based on motor errors. Our results uncover an important mechanism through which the human motor system can generate flexible and dextrous motor behaviour.

We carried out two experiments to examine the mapping of motor memories to control points. In experiment 1, we examined the ability of participants to learn opposing dynamics when they are associated with either different control points or a single control point. We then examined the reference frame in which control points are represented by testing generalization of learning. In experiment 2, we tested whether the assignment of separate memories to control points is obligatory or whether this only occurs when necessary.

Participants grasped the handle of a robotic interface (Fig. 1a), and a semi-silvered mirror was used to display a rectangular virtual object centred on the hand. The object translated with the hand. The workspace under the mirror was illuminated so that both the hand and the object were always visible (Fig. 1b). The object had three visible control points: circles displayed on the left and right of the object and a cross at the centre of the object. For participants in the two-control-points group ($n = 10$), a target appeared above one of the two lateral control points at the start of each trial and participants were instructed to move the corresponding control point to the target (Fig. 1c). The target location (left or right) cued the direction of the force field on exposure trials (see below). For

participants in the single-control-point group ($n=8$), a central target appeared above the central control point and participants were instructed to move the central control point to this target (Fig. 1d). In this group, as in the two-control-points group, a lateral 'target' was also displayed to cue the direction of the force field. Crucially, for both groups, the start position of the hand and the required final position of the hand were the same in all trials.

In the pre-exposure phase, participants made movements in a null field. In the exposure phase, opposing force fields were associated with the two lateral targets. Hence, for participants in the two-control-points group, each force field was also associated with the point on the object that had to be controlled. To produce the same movement of the hand in both force fields, participants needed to learn the opposing dynamics.

Participants performed 52 blocks of 8 trials (416 trials) in the exposure phase with an equal number of trials for each target in a pseudorandom order. So that predictive force compensation could be assessed independently from co-contraction, one randomly selected trial in each block was a channel trial[25,35], in which the movement was confined to a simulated mechanical channel to the target. On these trials, the forces generated by participants into the wall of the channel could be measured.

To assess performance, we measured kinematic error, defined as the maximum perpendicular error (MPE), between the actual and ideal (that is, straight) hand path. We also measured force compensation on channel trials, defined as the percentage of the force required to fully compensate for the force field (adaptation). During the pre-exposure phase, as expected, the kinematic error and adaptation were close to zero (Fig. 1e,f). At the start of the exposure phase, the force fields produced substantial deviations of the hand path from a straight line (Supplementary Fig. 1). To assess learning, we compared adaptation, which unlike MPE is not influenced by stiffness, in the final two blocks of the pre-exposure and exposure phases. This revealed a significant interaction between group and epoch (mixed-design analysis of variance (ANOVA), $F_{1,16}=73.31$, $P=2\times10^{-7}$). Adaptation reached $68.1\pm6.6\%$ and $-0.2\pm4.3\%$ of full force compensation by the end of the exposure phase for the two- and single-control-point groups (Fig. 1f), respectively. For the two-control-points group, the increase in adaptation was significant (two-tailed paired t-test, $69.4\pm6.7\%$, $t_9=10.99$, $P=2\times10^{-6}$).

The failure to learn when controlling a single control point is consistent with previous studies showing that arbitrary visual cues do not facilitate learning of opposing force fields[28,29,36], and indicates that the learning observed when controlling two different control points—despite making similar hand movements—is not simply due to the contextual cues provided by the lateral targets.

We performed two additional control experiments. In the first (Supplementary Fig. 2), we show that participants ($n=8$) can learn opposing fields, linked to different control points, even when they are required to fixate a central fixation point. This rules out the possibility that learning is due to associating field direction with gaze position. The second control was designed to rule out the possibility that subjects might be treating the two control points (small circles) as separate objects, despite the fact that they move coherently and are bound by a rectangle. In this control, we used an object where the control points were defined by the geometry of the object and there were no distinct visual elements (Supplementary Fig. 3). We show that participants ($n=8$) can still learn opposing fields linked to these different control points (Supplementary Fig. 3).

Our hypothesis that separate memories can be formed for different control points on manipulated objects assumes that these points are represented in object-centred coordinates; that is, that translating the object would not interfere with the learned memories associated with these points. However, other interpretations are possible based on the results for the two-control-points group. Specifically, whereas our hypothesis assumes that memories formed for the two fields are linked to the locations of the control points relative to the object (object-centred representation), it is possible that these memories are linked to the locations of the targets relative to the body (body-centred representation) or the locations of the targets and control points relative to the hand (hand-centred representation).

Based on our hypothesis and pilot data, we anticipated that participants in the two-control-points group would learn the two force fields. Therefore, for this group only, we included a generalization phase following the exposure phase in which we tested the alternative interpretations outlined above. As shown in Fig. 1e,f, performance—measured by both the kinematic error and adaptation—was stable during this phase.

In the generalization phase, we used channel trials to measure the forces produced in four configurations (Fig. 2a) where: (1) the hand and object were in the original exposure configuration; (2) both the object and hand translated; (3) only the hand translated; and (4) only the object translated. Note that Fig. 2a shows the generalization trials involving the left target. In trials involving the right target, the hand and/or object were translated in the opposite direction. In all configurations, the object moved with the hand with the appropriate offset throughout the movement. Fig. 2b shows the direction of force we expect the participants to generate for each possible representation (that is, body-, hand- or object-centred) for each configuration. All predictions are for the case in which the left and right targets/control points were associated with clockwise (CW) and counterclockwise (CCW), respectively. In the exposure configuration, we expect participants to generate forces in the appropriate (in this case, leftward) direction, and this is consistent with all three possible representations (Fig. 2b, left). Importantly, however, the pattern across the other three configurations is different for each possible representation.

The thick black bars in Fig. 2c show the measured force compensation (signed adaptation) in all four configurations relative to the force required to fully compensate for the force field in the exposure configuration. The thin grey bars show the force compensation in trials involving the right target, in which all predicted forces were in the opposite direction. Separate t-tests revealed that adaptation was significantly different from zero for both the left and right targets in the object-and-hand (two-tailed one-sample t-test, left target: $32.6\pm9.2\%$, $t_9=3.75$, $P=0.005$; right target: $-48.0\pm8.3\%$, $t_9=6.12$, $P=2\times10^{-4}$) and hand translation configurations (two-tailed one-sample t-test, left target: $-34.4\pm5.9\%$, $t_9=6.14$, $P=2\times10^{-4}$; right target: $34.5\pm5.0\%$, $t_9=7.28$, $P=5\times10^{-5}$). Furthermore, the direction of adaptation in these configurations was only consistent with the object-based predictions. Although adaptation was not significantly different from zero for either target in the object translation configuration (two-tailed one-sample t-test, left target: $12.5\pm6.5\%$, $t_9=2.03$, $P=0.072$; right target: $-3.5\pm9.9\%$, $t_9=0.38$, $P=0.714$), the sign of adaptation was again consistent with the object-based predictions. Note that the magnitude of force compensation (that is, length of the bars) relative to the exposure configuration decreased in all three generalization configurations, involving translation of the hand and object, object or hand. This decrease is consistent with a large body of literature showing that motor learning is generally local, with graded reduction with changes in context[2,37]. Overall, these results clearly support the hypothesis that separate memories are formed for control points represented in object-centred coordinates.

Having established that participants can form separate motor memories for different control points, we asked whether this process is obligatory or flexible. Specifically, we tested whether separate memories are formed even when the dynamics experienced for the different control points is the same. In contrast with experiment 1, here, a single motor memory would be sufficient for representing the dynamics of both control points and would also support

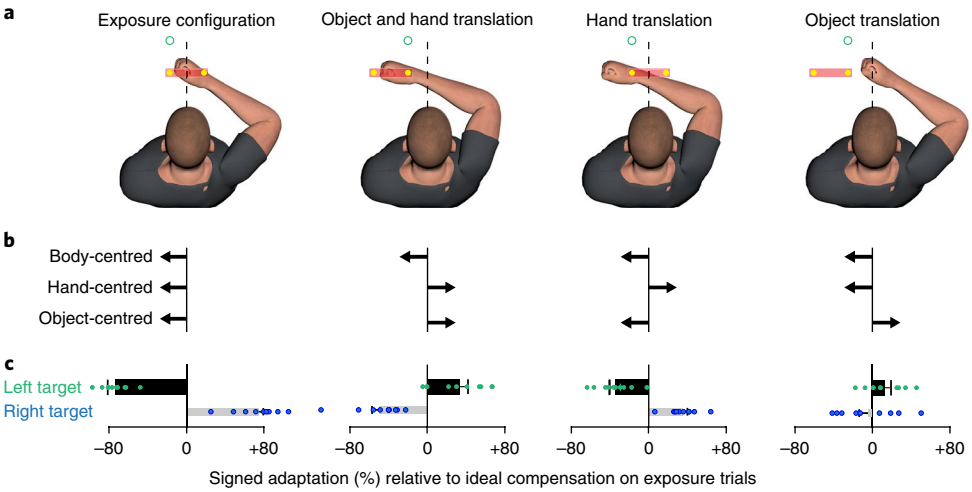

Fig. 2 | Control points are represented in an object-centred frame of reference. a, Configurations used to examine generalization of learning for trials with the left target. For trials with the right target all translations were reversed. All these trials were channel trials. **b**, Predictions of the direction of force according to the three possible representations. Note that these are for the scenario in which the left and right targets/control points were associated with the CW and CCW fields, respectively. The predictions for the right target (not shown) are in the opposite directions. **c**, Mean + s.e.m. signed adaptation across participants ($n = 10$) relative to the ideal compensation on exposure trials. The sign of the bar (+ or −) indicates compensatory forces appropriate for CCW and CW fields, respectively. Black and grey bars correspond to trials with the left and right targets, respectively. Dots represent data from individual participants.

efficient allocation of neural resources. Two groups were examined: participants in the opposing-field group ($n = 8$) experienced a different (opposing) force field for each control point, whereas participants in the same-field group ($n = 8$) experienced the same force field for each control point. To assess the separation of motor memories, after learning we de-adapted one control point with null-field trials and then assessed the state of adaptation when controlling the other control point (Fig. 3). If the memories are separate, de-adapting one control point should not de-adapt the memory for the other control point.

Both groups learned to compensate for the perturbation (Fig. 3a,c, MPE; Fig. 3b,d, adaptation) and, as expected, learning was greater for the group who learned the same field for both control points. By the final block of the exposure phase, there was no significant difference in adaptation between the opposing-field group ($52.8 \pm 12.1\%$) and the two-control-points group (experiment 1) ($68.9 \pm 5.9\%$) who performed the same task (two-tailed unpaired t-test, $16.1 \pm 13.1\%$, $t_{16} = 1.27$, $P = 0.222$). To assess whether de-adapting one memory led to de-adaptation of the other memory, we compared the mean of the last two channel trials in the post-exposure phase for the first control point with the first channel trial in the post-exposure phase for the second control point. For the group who learned opposing force fields, after de-adapting one control point, substantial adaptation re-emerged (Fig. 3b; two-tailed paired t-test, $37.6 \pm 8.6\%$, $t_7 = 4.69$, $P = 0.002$) when controlling the other control point. Although this effect is primarily driven by the first channel trial, this first trial provides a critical test for the separation of memories. This suggests that separate representations existed for each control point. In contrast, for the group that experienced the same force field for both control points, when we de-adapted one control point there was minimal adaptation remaining (Fig. 3d; two-tailed paired t-test, $9.4 \pm 7.8\%$, $t_7 = 1.31$, $P = 0.232$) when switching to the other control point. This was despite the greater adaptation observed in the same-field group, which increased the power to detect a difference in adaptation between the two control points during de-adaptation. This suggests that a single representation existed for both control points in this case.

We fit several candidate models to the data and performed model comparison. Context-dependent SSMs have been used to account for motor learning of opposing perturbations[38–40]. Briefly, these models assume that each context (force field) is associated with separate states of adaptation that are updated based on the error from the previous trial. Contexts can be coupled such that errors in one context update the states associated with the other context, and states associated with both contexts contribute to the final output. However, critically, these models assume that the coupling between contexts is known in advance and remains fixed over time. Therefore, they predict that: (1) with no coupling, two separate memories will be formed; (2) with complete coupling, a single memory will be formed; and (3) with partial coupling, two overlapping memories will be formed. While it is difficult to account for our results with either no coupling or complete coupling, it is possible that a context-dependent SSM with partial coupling could explain the data.

Context-dependent SSMs can be either single-rate[33,41] or dual-rate, in which the total adaptation involves two memory processes: (1) a fast process that both adapts and decays quickly; and (2) a slow process that adapts and decays more gradually[24,42]. We examined seven variants of the context-dependent SSM (Supplementary Table 1)[38,40], which vary as to whether single- or dual-rate states are included and also which states are coupled (see Methods for details).

As an alternative, we also developed a normative SSSM[43–45] of motor learning. The SSSM is a generalization of the SSM to systems with multiple operating modes (here, contexts), each of which can be associated with different, and even evolving, dynamics. On each trial, the system is in one context that determines both the dynamics experienced and the cues observed. Between trials, contexts switch stochastically. On each trial, the learner must infer the probability of each context (from control-point cues and prediction errors) and use this information to partition control and learning between two context-specific dual-rate states (see Methods for details). Importantly, although the association between cues and contexts is deterministic (the control point perfectly predicts the force-field direction), this association must be learned through experience. We therefore reasoned that the formation of separate motor memories may arise from participants learning the association between cues and contexts. Critically, in the SSSM, the probabilities of cues (control points) given contexts (force fields) are therefore learned online.

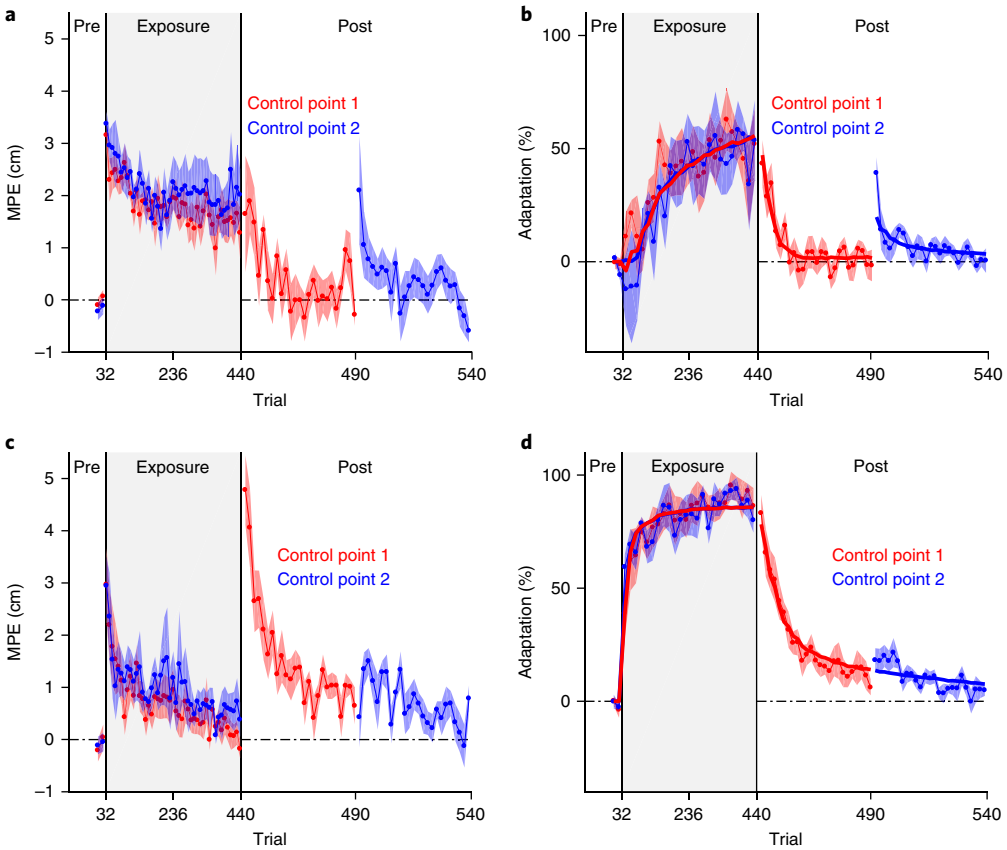

Fig. 3 | The encoding of dynamics for different control points depends on the fields experienced. a,**b**, MPE ± s.e.m. (**a**) and adaptation ± s.e.m. (**b**) for each control point in the group that experienced opposing force fields at each control point ($n = 8$). Data in the pre-exposure (Pre) and exposure phases were first averaged over blocks of eight trials. The post-exposure phase (Post) has been expanded for clarity. For simplicity, the sign of adaptation for control point 2 has been inverted. **c**,**d**, Same as **a** and **b**, respectively, but for the group that experienced the same force field at each control point ($n = 8$). Solid lines in **b** and **d** show the mean SSSM fits across participants.

We fit each model to the data from both the opposing- and same-field groups simultaneously, and performed model comparison using the Bayesian information criterion (BIC) (Supplementary Table 2). Although the context-dependent SSMs qualitatively capture the difference in post-washout adaptation between the same- and opposing-field groups (Supplementary Fig. 4), the SSSM fits the overall time course of adaptation and de-adaptation in the opposing-field group better (Fig. 3b,d, solid lines; slow and fast states shown in Supplementary Fig. 5) and has much stronger support (ΔBIC of 112.4 relative to the next-best model).

To understand how the SSSM works, we examined how the estimated probability of each context given a cue evolves for each group. As shown in Fig. 4, at the start of the experiment both contexts are activated equally by the right control point (that is, the probability of each context given the right control point is 0.5). Therefore, the model starts naive with respect to how control points relate to contexts. In the same-field group, both contexts are activated equally throughout the experiment, regardless of the control point, leading effectively to a single motor memory. In contrast, in the opposing-field group, each context becomes paired with a different control point, resulting in separate motor memories.

Our results demonstrate that the motor system can form separate memories for different control points on the same object, even when the movements associated with these points are the same. By examining generalization, we found that learning was associated with control points on the object and not with the location of the object in extrinsic space or the location of the control point relative to the hand. Moreover, we found that the motor system only forms distinct memories if the dynamics of the control points differs, allowing efficient and flexible allocation of motor memory. Finally, we developed a normative model of context-dependent

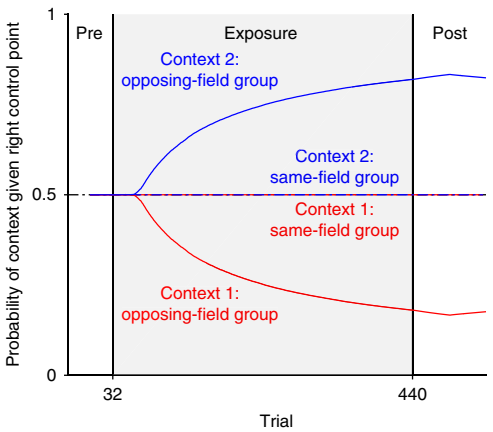

Fig. 4 | Learning to associate contexts with cues in the SSSM. The SSSM estimates the probability of each context given the cue (plotted here for the right control point cue before movement). Following exposure to opposing force fields, participants learn to differentiate between the two contexts given the right control point. Participants trained on the same force field at each control point do not learn to differentiate between contexts, leading to a single motor memory. Traces show mean model fits across participants. The plot for the left control point (not shown) is the mirror image about the line 0.5.

motor adaptation that can account for such flexible parcellation of motor memories.

Humans have a remarkable capacity to manipulate objects with different dynamics, and a central focus of research in motor control has been to elucidate how the brain learns and represents these dynamics. To investigate how contextual information can be used to learn different dynamics, numerous studies have used opposing novel dynamics (for example, viscous curl fields) that perturb the hand in opposite directions. This work has shown that the ability to learn opposing dynamics, when each is associated with a visual cue, such as the colour of the cursor or background, is generally highly limited[28,29,36]. Similarly, when lifting physical objects with different mass distributions, substantial interference is observed when each mass distribution is associated with a different visual geometric cue[12,13]. In agreement with these findings, we show that when controlling a single control point, participants cannot learn opposing fields when they are associated with the location of peripheral visual cues that correspond to the targets in the two-control-points group.

Several studies have shown that opposing fields can be learned if the perturbed movement is preceded or followed by a separate movement that differs for each field, or if the perturbed movement is accompanied by a concurrent movement of the other hand that again differs for each field[23,36,46–48]. Furthermore, previous studies have shown that opposing fields can be learned if they are associated with different states of the limb, as when the arm operates in a different region of the workspace for each field[29,49–51] or a visual–proprioceptive discrepancy is introduced so that the perceived state of the limb is different for each field[29,52]. Critically, in our experiment, and in contrast with these previous studies, veridical visual feedback of the hand was provided throughout the movement, and the movement start and end points were the same for the opposing fields. Consequently, participants' estimates of the state of the limb did not differ for the two fields. Therefore, we can be confident that it is the control of different points on the object that allows the formation of separate memories for different dynamical contexts. Moreover, we show clearly that the learning of each control point is linked to the location on the object.

Tool use generally involves controlling a specific location, or 'control point', on the tool as it interacts with the environment, such as the face of a hammer striking a nail or the eraser of a pencil rubbing a page. Skilled performance when using tools requires knowledge of the dynamics of the tool (relating applied force to motion) as well as contact mechanics[53,54], which may vary across control points. Most natural manipulation tasks involve a series of action phases separated by contact events[4,11]. Consider, for example, grasping a pencil, lifting it out of a container and transporting it to a piece of paper, using it to erase a pencil mark and then replacing it in the container. Here, contact between the fingertips and pencil marks the end of the reach phase, contact between the pencil and paper marks the end of the transport phase, the breaking of contact between the pencil and paper marks the end of the erase phase, and so on. By comparing predicted and actual sensory signals associated with these contact events, the motor system can monitor task progress, launch corrective actions as needed, and calibrate internal models of objects and their interactions[4,11]. Critically, both the control point on the object and the dynamics may change from phase to phase. For example, while erasing, the eraser end of the pencil is controlled and the dynamics includes the friction between the eraser and paper. The ability to form separate motor memories for different control points may thus be an essential component of skilled object manipulation and tool use.

Recent studies in neurophysiology, neuroimaging and neuropsychology support the idea that tools are incorporated into a body schema. For example, monkeys have been trained[55] to use a rake to retrieve a pellet of food that could not be reached by hand. Following tool use, the visual receptive fields of intraparietal neurons expanded beyond the space surrounding the hand to include the tip of the rake. Similar incorporation of tools is supported by studies in humans making temporal order judgements of tactile stimuli on the hand[56]. Importantly, such incorporation is seen only for the functional part of a tool[57] and a tool must be actively controlled for assimilation to occur[55,58]. This suggests that the point being controlled on a tool determines how the body schema changes with tool use. Interestingly, the body schema is thought to consist of distinct neural modules that represent different body parts[59,60]. It is therefore conceivable that different control points are assimilated by different body schema modules. Indeed, one may expect to find intraparietal neurons that respond differently for different control points on a tool. Furthermore, following incorporation of control points into the body schema, the effective 'state' of the body may include the control point, allowing different dynamics to be associated with different states linked to control points.

We found that the formation of distinct motor memories for different control points is not obligatory, but only occurs if the dynamics for each control point is different. Therefore, the allocation of motor memory is both flexible and efficient. To explain this result, we developed a model of motor adaptation based on an SSSM[43–45], which is a generalization of the mixture-of-experts architecture in neural networks[61,62] to dynamical systems[63]. The SSSM is, unlike these previous models, normative and therefore derived from first principles. Moreover, although the context-dependent SSMs could qualitatively capture the difference in post-washout adaptation between the same- and opposing-field groups, model comparison convincingly selected the SSSM over existing models. SSSMs combine a hidden Markov model with linear dynamical systems and can be used to model systems with multiple discrete operating regimes, termed modes. An SSSM with one mode is an SSM. The key innovation of the SSSM is that only one of the state-space modes is active at any one time and, over time, the system can transition between modes. For example, an SSSM would be appropriate when handling different objects. The transition between the use of different objects can be considered as a Markov process specifying the probability of switching from one object to another (for example, from kettle to cup) and the dynamics of each object can be different and change over time (for example, as the kettle empties and the cup fills).

Within this framework, the problem for the sensorimotor system in our experiment is twofold. First, it must infer the current mode (for example, the context) and the state of the dynamics (for example, the force-field perturbation) based on the parameters of the SSSM. The expected perturbation is then a weighted sum of the perturbations expected for each mode, with weights given by the probability of each mode. Second, it must update the parameters of the SSSM online to ensure that these inferences are as accurate as possible. Here, we provide evidence to support the idea that motor adaptation involves not only state inference but also parameter learning or system identification[64–67].

For simplicity, the SSSM we used had two modes. However, in general, SSSMs can have any number of modes. Central to the performance of the model here is its capacity to learn through experience (that is, during the experiment) the associations between cues (for example, control points) and contexts (for example, force fields) via online parameter estimation. To reduce the degrees of freedom of the model, we restricted the simulation to only update the parameters that determine the probabilities of the cues given the contexts. However, in general, all parameters of the model can be updated online. The fits of the SSSM suggest that participants only develop distinct memories for each control point if the dynamics are different (Fig. 4). In non-parametric extensions of the standard SSSM, the number of modes is learned through experience, rather than fixed a priori[68]. Such a model would allow the motor system to be efficient by recruiting additional context-dependent memories (that is, modes) when control points have different dynamics

and, conversely, removing modes that are redundant when control points have the same dynamics.

Our results suggest that objects are not represented by the motor system as holistic entities, but are instead parcellated in a task-dependent manner according to control points. Interestingly, the results of the SSSM suggest that effective contextual cues, such as control points, do not necessarily engage distinct motor memories a priori. Instead, they engage online parameter-learning processes that form distinct motor memories only if and when needed.

Methods

Participants. A total of 50 neurologically intact participants (22 males and 28 females; age 28.2 ± 7.8, mean ± s.d.) were recruited to participate in four experiments, which had been approved by the Cambridge Psychology Research Ethics Committee. All participants provided written informed consent and were right-handed according to the Edinburgh handedness inventory[69].

Experimental apparatus. All experiments were performed using a vBOT planar robotic manipulandum with a virtual-reality system and air table[70]. The position of the handle was measured using optical encoders sampled at 1 kHz, and torque motors allowed forces to be generated on the handle. A monitor mounted above the vBOT projected virtual images into the plane of movement via a horizontal semi-silvered mirror (Fig. 1a). Participants were seated in front of the vBOT and grasped its handle with their right hand. A lamp was used to illuminate the hand below the mirror with the illumination adjusted so that both the vBOT, hand, arm and virtual images were clearly visible (Fig. 1b). This was done to ensure that participants always had an accurate estimate of the state of their hand and arm. The right forearm was supported on an air sled, which constrained arm movements to the horizontal plane and reduced friction.

On each trial, the vBOT could generate forces associated with either a velocity-dependent curl field (force-field trials) or a force channel (channel trials). Alternatively, in the case of the null field, no forces were generated (null-field trials). For the curl field, the force generated on the hand was given by

$$\begin{pmatrix} f_x \\ f_y \end{pmatrix} = g \begin{pmatrix} 0 & -1 \\ 1 & 0 \end{pmatrix} \begin{pmatrix} \dot{x} \\ \dot{y} \end{pmatrix} \quad (1)$$

where f_x, f_y, $\dot{x}$ and $\dot{y}$ are the forces and velocities at the handle in the x and y directions (mediolateral and anteroposterior, respectively). The field gain g was set to ±15 N s m^{-1} and the sign of g specified whether the curl field was CW or CCW. On channel trials, the hand was constrained to move along a straight line to the target. This was achieved by simulating forces associated with a stiff spring and damper, with the forces acting perpendicular to the long axis of the channel. A spring constant of 6,000 N m^{-1} and a damping coefficient of 5 N s m^{-1} were used. Channel trials allowed the feedforward forces generated by participants to be measured orthogonal to the direction of reach[25,35].

In all experiments, participants first performed a familiarization phase of between 96 and 128 trials, consisting of null-field trials and channel trials for each control point in a pseudorandomized order.

To have precise control over vision and dynamics in our experiment, we used a robotic interface and virtual-reality system. Importantly, a number of previous object-manipulation studies using robotic manipulanda have been shown to produce similar results to experiments that use real-world physical objects[5,12,32,70,71].

Experiment 1: encoding of motor memories by control points. *Two-control-points condition.* In the two-control-points condition, we investigated whether participants could learn opposing (CW and CCW) force fields when each field was associated with a different control point on the object. The paradigm consisted of pre-exposure, exposure, generalization and de-adaptation ('washout') phases, as detailed below.

Pre-exposure, exposure and de-adaptation phases. Participants (n = 10) grasped the handle of the vBOT and a virtual object (solid red rectangle of 16 cm × 3 cm) was displayed centred on the hand (Fig. 1b). The position of the object translated with the hand. The object had two potential control points (green discs with a radius of 0.4 cm) ±7 cm lateral to the centre of the object.

To start each trial, participants aligned the centre of the object (indicted by a yellow cross) with the home position (a circle with a radius of 0.5 cm) situated in the midline approximately 30 cm in front of the participant's chest. The trial started after the centre point was within 0.3 cm of the home position and had remained below a speed of 0.5 cm s^{-1} for 100 ms. After a 0.2 s delay, a target (a circle with a radius of 0.5 cm) appeared 12 cm away (anteriorly along the y axis) above either the left or right control point. A tone indicated that the participants should initiate a reaching movement to the target. Participants were instructed to move the corresponding control point to the target. That is, if the target was aligned with the left control point, they should move the left control point to the target, and conversely for the target aligned with the right control point. Crucially, because each target was aligned with its respective control point, the hand moved to the same location to attain both targets.

A trial ended when the control point had remained within 0.3 cm of the target for 50 ms. If the peak speed of the movement was less than 50 cm s^{-1} or more than 70 cm s^{-1}, a low-pitch tone sounded and a 'too slow' or 'too fast' message was displayed, respectively. At the end of each trial, the vBOT actively returned the hand to the home position.

After familiarization, participants performed blocks of eight trials in which one of the trials (not the first) was randomly chosen as a channel trial and the remainder were either null-field trials or force-field trials. The paradigm consisted of a pre-exposure phase (4 blocks/32 trials), an exposure phase (52 blocks/416 trials), a generalization phase (71 blocks/568 trials; see below) and a de-adaptation phase (12 blocks/96 null-field trials). Each target appeared an equal number of times within a block in a pseudorandom order.

During the exposure phase, the location of the target (left or right) determined the direction of the force field (CW or CCW) applied during the movement. As such, the field direction was associated with the particular control point on the object (left or right) and its corresponding target (Fig. 1c). The direction of the force field for each control point was counterbalanced across participants. A 45 s rest break was given after blocks 12, 25, 38 and 51 of the exposure phase.

Generalization. The generalization phase (immediately after the exposure phase) was used to investigate the representation of the memories for the two force fields. Specifically, we tested whether the representations were object-centred (associated with the location of the control points on the object), body-centred (associated with the locations of the targets/control points relative to the body) or hand-centred (associated with the location of the targets/control points relative to the hand). The generalization phase included force-field trials (to maintain adaptation), as well as channel trials (to monitor ongoing adaptation and examine generalization). To monitor adaptation, participants performed channel trials with the hand and object in the original exposure configuration. To examine generalization, participants performed channel trials during lateral translations (±14 cm) of either the object or the hand, or both the object and the hand. This gave three kinds of generalization trial (Fig. 2a).

On object-and-hand translation trials, participants translated the hand and the object ±14 cm along the x axis before the trial started. For leftward translations of the object and hand, the left target was cued and the participant moved the right control point toward the target (which was now aligned with the left target). The converse was true for rightward translations. Importantly, as on all trials in the study, the control points and targets were always aligned along the y axis, thus requiring a straight movement.

On hand translation trials, participants translated their hand ±14 cm along the x axis while the object remained in the centre of the workspace. For leftward translations of the hand, the left target was cued and the participant moved the left control point toward the target. The converse was true for rightward translations.

On object translation trials, the object was visually translated ±14 cm along the x axis while the hand remained in the centre of the workspace. For leftward translations of the object, the left target was cued and the participant moved the right control point toward the target. The converse was true for rightward translations.

In all conditions, the object tracked the hand during the movement with the fixed offset associated with the particular generalization type maintained throughout the trial.

A 2.5 s delay was imposed at the start of each channel trial to allow time for the participant to translate their hand and/or the object, if required. A 15 s rest break was given every 9 blocks during the generalization phase starting at block 8. A block of force-field trials (with no channel trials) followed each rest break to mitigate the effects of any time-dependent decay of motor memory. Each of the channel types (2 to monitor ongoing adaptation and 6 for generalization) was repeated 8 times and there were 7 pure exposure blocks post-rest, giving 71 blocks (568 trials).

Note that the familiarization phase in the two-control-points condition included trials for each of the generalization conditions described above.

Single-control-point condition. In the single-control-point condition, we examined whether the visual targets alone could provide a contextual cue for learning. A separate group of participants (n = 8) performed the single-control-point condition task. As for the two-control-points condition (described above), the left and right control points were displayed on the object. Similarly, the left and right targets were displayed and were always associated with the particular field direction (CW or CCW). However, participants were instructed to move the central control point (yellow cross) on the object to a central target (which remained on the screen at all times) (Fig. 1d) and to ignore the lateral targets. Participants were thus required to control a single control point. The paradigm consisted of the same pre-exposure (4 blocks/32 trials), exposure (51 blocks/408 trials) and de-adaptation (12 blocks/96 trials) phases as for the two-control-points condition. However, in this condition the generalization phase was omitted.

Gaze fixation control. During target-directed reaches, people tend to fixate the target[72–74]. The gaze fixation experiment ($n=8$) was performed to exclude the possibility that gaze direction, rather than the control point on the object, was the contextual cue responsible for adaptation to opposing force fields.

An EyeLink 1000 eye tracker was used to track the position of the left eye at 500 Hz. The eye tracker was mounted at an oblique angle between the handle of the manipulandum and a transparent reflective sheet of plastic that was used to project visual feedback (replacing the semi-silvered mirror). A forehead rest was used to stabilize the head. The eye tracker was calibrated at the start of the experiment and after every rest break using a nine-point grid.

The paradigm included both fixation and free-gaze trials. On fixation trials, participants had to fixate a small cross (located 8 cm above the home position) while performing the task (moving the left or right control point to the left or right target, respectively). Because movements were guided by peripheral vision, the spatial tolerance of the target was increased to 0.6 cm. If the participant broke fixation (>2 cm), the trial was aborted and repeated. The central control point on the object was not displayed to prevent participants from using it to guide the movement towards the fixation point. The home position was indicated by a rectangular frame that was visible at all times during the experiment. On free-gaze trials, no fixation cross was displayed and eye movements were unconstrained.

After familiarization (described above), participants performed a fixation pre-exposure phase (4 blocks/32 trials), a fixation exposure phase (65 blocks/520 trials), a free-gaze exposure phase (64 blocks/512 trials) and a free-gaze de-adaptation phase (12 blocks/96 trials). The direction of the force field associated with each control point was counterbalanced across participants. Each block had the same structure as for the two-control-points condition, with seven exposure trials and one channel trial.

A 45 s rest break was given every 13 blocks during the exposure phase starting at block 12. A block of force-field trials (with no channel trials) followed each rest break to mitigate the effects of any time-dependent decay of motor memory.

Uniform object control. The object used in the main experiment consisted of different visual elements (green circular control points embedded in a red rectangle) that could conceivably be interpreted as distinct objects. We therefore repeated the exposure phase in the two-control-points group using an object that no longer contained different visual elements. A separate group of participants ($n=8$) controlled a new uniform object with control points that were not discriminable from the rest of the object by colour (Supplementary Fig. 3). The red rectangle was removed from the original object and the control points (green discs with a radius of 0.4 cm) were connected by a bar (solid green rectangle of 14 cm × 0.6 cm) that was the same colour as the control points. Importantly, these control points were the same size and in the same location as those of the original experiment. We reduced the size of the central cross so that it would fit inside the connecting bar.

As in the two-control-points experiment (described above), participants moved the corresponding control point to the displayed target, which was always associated with a particular field direction (CW or CCW). The paradigm consisted of the same pre-exposure (4 blocks/32 trials), exposure (51 blocks/408 trials) and de-adaptation (12 blocks/96 trials) phases as in the single-control-point experiment.

Experiment 2: are separate motor memories obligatory for different control points? This experiment was performed to investigate whether separate motor memories are formed even when the dynamics experienced at the two control points on the object are the same.

After familiarization, participants performed a pre-exposure phase, an exposure phase and a de-adaptation phase. The pre-exposure (4 blocks/32 trials) and exposure phases (51 blocks/408 trials) were the same as in experiment 1. Participants performed blocks of eight trials consisting of seven null (pre-exposure) or field (exposure) trials and one channel trial. In the exposure phase, half the participants ($n=8$) experienced opposing fields at each control point (as in experiment 1) and the other half ($n=8$) experienced the same field at each control point. In both the opposing-field and same-field conditions, the direction of the force field for each control point was counterbalanced across participants. A 45 s rest break was given after blocks 12, 25 and 38 of the exposure phase. A block of force-field trials (with no channel trials) followed each rest break to mitigate the effects of any time-dependent decay of motor memory.

The exposure phase was followed by 50 blocks of de-adaptation, with each block consisting of 1 null-field trial and 1 channel trial. Importantly, one control point was cued throughout the first half of the de-adaptation phase (the first 25 blocks/50 trials) and the other control point was cued throughout the second half (the last 25 blocks/50 trials). The order in which each control point (left or right) was cued was counterbalanced across participants.

If the dynamics at both control points is encoded by a single representation, de-adaptation at one control point should also lead to de-adaptation at the other control point. Alternatively, if the representations are separate, de-adaptation at one control point should have minimal effect on the representation associated with the other control point.

Data analysis. Data analysis was performed using MATLAB R2017a. Two measures of performance were calculated. On null-field and force-field trials, we calculated the maximum distance between the path of the hand and a straight line connecting the start position and the target (that is, the MPE). On channel trials, we calculated the percentage of the force field that was compensated for (adaptation) by regressing the actual forces $f_a(t)$ generated by participants in the channel on the ideal forces $f_i(t)$ that would fully compensate for the forces on a force-field trial (defined in equation (1)):

$$f_a(t) = b \times f_i(t) \tag{2}$$

$$\text{adaptation} = b \times 100\% \tag{3}$$

where b is the regression coefficient and t is the discrete time step in the trial. The offset of the regression was constrained to zero. For this analysis, we used the portion of the movement where the hand velocity was greater than 1 cm s^{-1}. To combine MPE and adaptation results across participants, data from individual participants were signadjusted according to the direction of the field.

To identify changes in MPE and adaptation within and between experiments, mixed-design ANOVAs and paired t-tests were performed. Comparisons of the final level of adaptation between experiments were performed using between-subjects ANOVAs and unpaired t-tests. All statistical tests were two-sided with significance set to $P<0.05$. Where values are reported, they represent the mean ± s.e.m.

Models. We fit two classes of model to experiment 2. The first class was a deterministic, context-dependent SSM based on refs [38–40]. The second class was a probabilistic SSSM. We did not fit the models to experiment 1 as this experiment was not designed to distinguish between the model classes. Note, however, that the initial part of experiment 1 was identical to the initial part for the opposing-field group in experiment 2.

Context-dependent SSM. We used a context-dependent SSM that included separate states for different contexts and also different rates of adaptation (slow versus fast adaptive processes). In the current study, there were two contexts (the left and right control points) and each context could include states that updated with slow and fast rates. This gave a total of four states (two contexts and two rates) that could be represented by the elements of a state vector

$$\boldsymbol{x} = \begin{pmatrix} x_s^{(1)} & x_f^{(1)} & x_s^{(2)} & x_f^{(2)} \end{pmatrix}^{\mathrm{T}} \tag{4}$$

where the superscripts represent which context the state is associated with (for example, 1 = left and 2 = right control points), the subscripts represent the slow (s) and fast (f) adaptation processes, and T is the tranpose operator. The motor output on trial t was a weighted sum of the elements in the state vector, with the weighting determined by the context:

$$y(t) = \boldsymbol{x}(t)^{\mathrm{T}} \cdot \boldsymbol{c}(t) \tag{5}$$

where the context weighting vector, $\boldsymbol{c}$, varies according to the context for the trial (left or right control point). The error on a trial is the difference between the motor output and the task perturbation:

$$e(t) = f(t) - y(t) \tag{6}$$

In the current study, the task perturbation, f, is zero for null-field trials, +1 for CW field trials and −1 for CCW field trials. The state vector is updated across trials:

$$\boldsymbol{x}(t+1) = \boldsymbol{a} \odot \boldsymbol{x}(t) + e(t) \cdot \boldsymbol{b} \odot \boldsymbol{c}(t) \tag{7}$$

where ⊙ represents element-wise multiplication. Trial-by-trial decay is determined by the retention vector $\boldsymbol{a}$. Error-dependent adaptation of states is determined by the context weighting vector and the learning-rate vector $\boldsymbol{b}$.

We considered seven variants of the model which determine the way $\boldsymbol{a}$, $\boldsymbol{b}$ and $\boldsymbol{c}$ are parameterized (Supplementary Table 1). The models vary as to whether there is a single context-dependent state (SSM 1), a slow/fast context-independent state and a fast/slow context-dependent state (SSMs 2–4), or both fast and slow context-dependent states (SSMs 5–7). For context-dependent states, the values in the context weighting vector determine the coupling (if any) between contexts. Models that include the parameters c_s and c_f can have coupling between the contexts for the slow and/or fast processes, respectively.

SSSM. *The generative model.* Here, we develop a probabilistic SSSM that allows the sensorimotor system to optimally partition learning across contexts. We assume that the environment consists of distinct contexts that switch in a probabilistic manner according to a hidden Markov model (Supplementary Fig. 6). Each context is associated with its own perturbations, which evolve according to linear-Gaussian dynamics. We assume that participants possess an internal generative model of perturbations that matches the environment. We characterize this model as an

SSSM—a generalization of the SSM to systems with multiple operating regimes or modes. SSSMs define a probability density over a time series of discrete and continuous states. Here, the discrete states represent contexts and the continuous states represent perturbations. We implement the model with two contexts, although the extension to more than two contexts is straightforward.

On trial t, the environment is in one of two contexts, $c_t \in \{1, 2\}$, and between trials the context either remains the same or switches in a stochastic manner. The context transition probabilities are defined by the matrix $\mathbf{\Pi}$, where

$$\pi_{ij} = p(c_t = j | c_{t-1} = i) \tag{8}$$

To reduce the number of free parameters in the model, we assume that the context remains the same or switches with equal probability; that is, $\pi_{ij} = 0.5$ for all i, j. This is consistent with the exposure phase of our experiment in which each force field is presented with equal frequency and in a pseudorandom order.

On trial t, the context gives rise to one of two observable cues, $q_t \in \{1, 2\}$, corresponding to the location of the control point. The cue emission probabilities are defined by the matrix $\mathbf{\Phi}$, where

$$\phi_{kj} = p(q_t = k | c_t = j) \tag{9}$$

The perturbations in each context evolve independently according to linear-Gaussian dynamics, as defined by the state transition function

$$\boldsymbol{x}_{t+1} = \boldsymbol{A}\boldsymbol{x}_t + \boldsymbol{w}_t \tag{10}$$

where $\boldsymbol{x}_t = \begin{pmatrix} x_{s,t}^{(1)} & x_{f,t}^{(1)} & x_{s,t}^{(2)} & x_{f,t}^{(2)} \end{pmatrix}^{\mathrm{T}}$ is a vector of slow and fast states (subscripts) for contexts 1 and 2 (superscripts), $\boldsymbol{A}$ is a diagonal matrix of the form $\mathrm{diag}(a_s, a_f, a_s, a_f)$ and $\boldsymbol{w}_t$ is zero-mean Gaussian process noise with covariance $\boldsymbol{Q} = \mathrm{diag}(q_s, q_f, q_s, q_f)$. Thus, we implement a probabilistic context-dependent dual-rate model.

The context determines which perturbations are observed, as defined by the output function

$$y_t = \boldsymbol{h}^{(c_t)}\boldsymbol{x}_t + v_t \tag{11}$$

where $\boldsymbol{h}^{(1)} = (1\ 1\ 0\ 0)$ is the observation vector for context 1, $\boldsymbol{h}^{(2)} = (0\ 0\ 1\ 1)$ is the observation vector for context 2 and v_t is the zero-mean Gaussian observation noise with variance r.

State inference. To operate effectively, the sensorimotor system must keep track of perturbations in the environment, as well as the contexts in which they occur. However, both perturbations and contexts are latent variables, which must be inferred from a sequence of observations $\{q_{1:t}, y_{1:t}\}$. Several techniques have been developed to infer the joint state, $\{c_t, \boldsymbol{x}_t\}$, of an SSSM[43–45,63,75,76]. Here, we focus on a technique known as the generalized pseudo-Bayesian estimator of order 1 (GPB1; ref. [76]), which we adapt for an SSSM in which the context, c_t, emits observable cues q_t. The GPB1 is an assumed-density filtering method that approximates the exact posterior of the state (a mixture of Gaussians with m^l components, where m is the number of modes and l is the number of trials) with a single Gaussian.

To maintain an estimate of the state, two Kalman filters operate in parallel (Supplementary Fig. 6). Each filter has a different observation vector, $\boldsymbol{h}^{(j)}$ (defined above), and is thus specialized for a different context; all remaining parameters are the same for both filters. On trial t, both filters operate on the same Gaussian estimate of the continuous state from the previous trial, with mean $\hat{\boldsymbol{x}}_{t-1|t-1}$ and covariance $\boldsymbol{V}_{t-1|t-1}$, to generate a Gaussian estimate of the continuous state on the current trial, with mean $\hat{\boldsymbol{x}}_{t|t}^{(j)}$ and covariance $\boldsymbol{V}_{t|t}^{(j)}$. This produces a mixture of Gaussians with mixing weights given by the probability of each context $\gamma_t^{(j)}$. Because the number of possible context sequences doubles with every trial, the number of components in this mixture will also double if no approximations are made, making inference intractable. Therefore, after each trial, the mixture of Gaussians is approximated by a single Gaussian via moment matching (Supplementary Fig. 6), rendering inference tractable but approximate.

Upon observation of the contextual cue q_t, but before movement, the probability of each context (assuming equiprobable context transitions) is

$$\rho_t^{(j)} = \frac{\phi_{q_t j}}{\sum_{i=1}^{2} \phi_{q_t i}} \tag{12}$$

The predicted observation used for control is

$$\hat{y}_t = \sum_{j=1}^{2} \rho_t^{(j)} \hat{y}_t^{(j)} \tag{13}$$

where $\hat{y}_t^{(j)} = \boldsymbol{h}^{(j)}\hat{\boldsymbol{x}}_{t|t-1}^{(j)}$ is the observation predicted for each context. We assume that the predicted observation is expressed through a motor action that is corrupted by zero-mean Gaussian noise (see section 'Model fitting').

After the movement, the likelihood of the observation y_t given each context is

$$\lambda_t^{(j)} = \mathcal{N}(y_t | \hat{y}_t^{(j)}, \sigma_t^{2(j)}) \tag{14}$$

Here, we use $\mathcal{N}(y_t | \hat{y}_t^{(j)}, \sigma_t^{2(j)})$ to denote the probability density function for the normal distribution with mean $\hat{y}_t^{(j)}$ and variance $\sigma_t^{2(j)}$, where $\sigma_t^{2(j)}$ is the standard Kalman filter innovation covariance. The final probability of each context is given by Bayes' rule:

$$\gamma_t^{(j)} = \frac{\lambda_t^{(j)} \rho_t^{(j)}}{\sum_{i=1}^{2} \lambda_t^{(i)} \rho_t^{(i)}} \tag{15}$$

Finally, a single Gaussian estimate of the perturbations is obtained via moment matching:

$$\hat{\boldsymbol{x}}_{t|t} = \sum_{j=1}^{2} \gamma_t^{(j)} \hat{\boldsymbol{x}}_{t|t}^{(j)} \tag{16}$$

$$\boldsymbol{V}_{t|t} = \sum_{j=1}^{2} \gamma_t^{(j)} \{\boldsymbol{V}_{t|t}^{(j)} + [\hat{\boldsymbol{x}}_{t|t}^{(j)} - \hat{\boldsymbol{x}}_{t|t}][\hat{\boldsymbol{x}}_{t|t}^{(j)} - \hat{\boldsymbol{x}}_{t|t}]^{\mathrm{T}}\} \tag{17}$$

Parameter learning. To perform state inference, the sensorimotor system must set the parameters, $\boldsymbol{\theta} = \{\boldsymbol{A}, \boldsymbol{Q}, \boldsymbol{h}^{(1)}, \boldsymbol{h}^{(2)}, r, \mathbf{\Pi}, \mathbf{\Phi}\}$, of the SSSM. Importantly, these parameters need not be fixed but may be learned online. In general, the sensorimotor system could learn all of these parameters online. However, to reduce the degrees of freedom of the model for our dataset, we assume that the sensorimotor system only learns the cue emission probabilities and that all other parameter estimates are fixed.

To learn the cue emission probabilities, we perform expectation maximization (EM)—an iterative method for obtaining maximum-likelihood estimates of unknown parameters in probabilistic models involving latent variables[77]. We utilize an online formulation of EM that can be interpreted as a stochastic approximation recursion on the expected sufficient statistics. A detailed description of this method can be found in refs [78,79]. Here, we provide a brief outline as applied to our perturbation study.

The algorithm iterates between an E step, in which the joint probability of c_t and q_t is estimated, and an M step, in which the joint probability of c_t and q_t is normalized to obtain the probability of q_t given c_t.

Stochastic E step. The aim of the E step is to count the number of times that each value of c_t and q_t co-occur. If both c_t and q_t were known, this would involve summing (over trials) a count of these co-occurrences:

$$\boldsymbol{\mathcal{S}}_l = \sum_{t=1}^{l} \boldsymbol{S}_t(q_t, c_t) \tag{18}$$

where the matrix $\boldsymbol{S}_t(q_t, c_t)$ is the complete-data sufficient statistic for a multinomial distribution and has a single unity entry defined by the indicator function

$$s_t(q_t, c_t)_{kj} = \begin{cases} 1 & \text{if } q_t = k, c_t = j \\ 0 & \text{otherwise} \end{cases} \tag{19}$$

To avoid storing the entire history of sufficient statistics, this sum can be calculated in a recursive manner:

$$\boldsymbol{\mathcal{S}}_t = \boldsymbol{\mathcal{S}}_{t-1} + \boldsymbol{S}_t(q_t, c_t) \tag{20}$$

with $\boldsymbol{\mathcal{S}}_0$ initialized to a matrix of zeros. However, because c_t is a latent variable, this recursion must be modified in the following two ways. First, $\boldsymbol{S}_t(q_t, c_t)$ is estimated in the form of an expectation:

$$\mathbb{E}_{\hat{\boldsymbol{\theta}}_{t-1}}[\boldsymbol{S}_t(q_t, c_t) | q_{1:t}, y_{1:t}] = \sum_{j=1}^{2} \gamma_t^{(j)} \boldsymbol{S}_t(q_t, c_t = j) \tag{21}$$

where the hat notation is used to indicate an estimated value. Second, because of observation noise, the expectations in equation (21) will show trial-to-trial variability. Therefore, an adaptive stepsize, $\eta_t = \alpha/(\alpha + t - 1)$, is used to average the sequence of expectations and promote convergence[80]. Because the stepsize decreases to zero according to the requirements of stochastic approximation theory, $\sum_{t=1}^{\infty} \eta_t = \infty$ and $\sum_{t=1}^{\infty} \eta_t^2 < \infty$, the effects of noise are eliminated in the long run[81]. Increasing α slows the rate at which the stepsize decreases, placing greater weight on more recent observations compared with older observations. We treat α

as a free parameter of the model. Taken together, these two modifications lead to the following recursion:

$$\boldsymbol{\mathcal{S}}_t = (1-\eta_t)\boldsymbol{\mathcal{S}}_{t-1} + \eta_t \mathbb{E}_{\hat{\boldsymbol{\theta}}_{t-1}}[\boldsymbol{S}_t(q_t, c_t)|q_{1:t}, y_{1:t}] \quad (22)$$

which computes a running average of the expected complete-data sufficient statistics. It is useful to note that the convex combination in equation (22) ensures that all elements of $\boldsymbol{\mathcal{S}}_t$ sum to 1. As such, $\boldsymbol{\mathcal{S}}_t$ can be interpreted as an estimate of the joint probability of c_t and q_t, which is proportional to the expected number of times that each value of c_t and q_t co-occurred.

While it is possible to compute smoothed estimates of the complete-data sufficient statistics[82], exact computation of these smoothed estimates is intractable, requiring sequential Monte Carlo sampling techniques[83]. For simplicity, we only compute filtered estimates of the complete-data sufficient statistics, as in equation (21).

M step. To calculate $\widehat{\boldsymbol{\Phi}}_t$, we normalize $\boldsymbol{\mathcal{S}}_t$ by dividing each element by its corresponding column sum to ensure that the probability of either cue being emitted in each context is 1. Note that all elements of $\boldsymbol{\mathcal{S}}_t$ must be non-zero for the solution of the expectation maximization algorithm to be well defined (otherwise some probabilities will always remain zero). Therefore, we omit the M step for the first eight trials to ensure that both contextual cues have been observed.

Importantly, to infer the probability of each context given an observed cue, the model of how contexts emit cues (equation (9)) is inverted (equation (12)).

Model implementation. We applied the above inference and learning algorithms to a sequence of noiseless observations, $y_{1:t}$, assigned values of 0 (null-field trials) or ±1 (force-field trials), corresponding to the actual perturbations delivered by the robot. We also examined adding zero-mean Gaussian noise (variance r) to the delivered sequence of perturbations to include observation noise. However, because the actual observation noise that participants perceived is unknown to us, it must be marginalized out (for example, using Monte Carlo integration). The inclusion of observation noise also results in a stochastic objective function, which requires alternative parameter optimization techniques. For simplicity, we only report fits to noiseless observations as the addition of observation noise did not qualitatively change the model fit or the outcome of model comparison.

To update the estimate of the continuous state, we applied the standard Kalman filter recursive equations[84]. The prior estimate of the continuous state was initialized with mean, $\hat{\boldsymbol{x}}_{0|0}$, and covariance, $\boldsymbol{V}_{0|0}$, equal to zero and the mean steady-state covariance matrix across Kalman filters, respectively. The prediction error of each Kalman filter, $y_t - \hat{y}_t^{(j)}$, was set to zero on channel trials.

We set $\boldsymbol{h}^{(j)}$ and $\boldsymbol{\Pi}$ as described above and initialized $\widehat{\boldsymbol{\Phi}}_0$ as a symmetric matrix

$$\widehat{\boldsymbol{\Phi}}_0 = \begin{pmatrix} \beta & 1-\beta \\ 1-\beta & \beta \end{pmatrix} \quad (23)$$

where $\beta = 0.5 + \varepsilon$ and $\varepsilon = 10^{-6}$. Thus, the learner starts naïve with respect to how cues relate to contexts. $\widehat{\boldsymbol{\Phi}}_t$ was updated recursively using the online expectation maximization algorithm. The small amount of jitter ε, was added to allow symmetry breaking. We used $q_t = 1$ and $q_t = 2$ for the left and right control points, respectively.

Model fitting. We simulated each model separately for each participant using the particular sequence of cues they observed. We then calculated the mean model data across participants for each group and each control point. We assume that adaptation measured on channel trials represents predicted observations that have been corrupted by independent and identically distributed Gaussian motor noise. Maximum-likelihood estimates of the free parameters of the models (Supplementary Table 2) were therefore obtained by minimizing the sum-of-squared errors between the mean model data (equation (5) for the SSMs and equation (13) for the SSSM) and the mean experimental data measured on channel trials (b in equation (2)). As each model involved fitting both same- and opposing-field groups jointly with the same set of parameters, we chose to fit the mean adaptation data across participants to reduce variability in the dataset.

Model comparison. Model selection was performed using the BIC:

$$\mathrm{BIC} = n \cdot \ln[(1-R^2)/n] + k \cdot \ln(n) + \text{constant} \quad (24)$$

where n (204) is the number of data points, k is the number of free parameters and the constant does not depend on the model. The first term in the BIC penalizes underfitting, whereas the second term penalizes model complexity, as measured by the number of free parameters in the model. Taking the difference in BIC values for two competing models approximates half the log of the Bayes factor[85]. A BIC difference of greater than 4.6 (a Bayes factor of greater than 10) is considered to provide strong evidence in favour of the model with the lower BIC value[86].

Life Sciences Reporting Summary. Further information on experimental design is available in the Life Sciences Reporting Summary.

Code availability. The code used to generate the data in this study is available from the corresponding author on request.

Data availability. Data that support the findings of this study are available from the corresponding author on request.

Received: 4 October 2017; Accepted: 20 February 2018;
Published online: 9 April 2018

References

1. Shadmehr, R., Smith, M. A. & Krakauer, J. W. Error correction, sensory prediction, and adaptation in motor control. *Annu. Rev. Neurosci.* **33**, 89–108 (2010).
2. Wolpert, D. M., Diedrichsen, J. & Flanagan, J. R. Principles of sensorimotor learning. *Nat. Rev. Neurosci.* **12**, 739–751 (2011).
3. Johansson, R. S. & Westling, G. Roles of glabrous skin receptors and sensorimotor memory in automatic control of precision grip when lifting rougher or more slippery objects. *Exp. Brain Res.* **56**, 550–564 (1984).
4. Johansson, R. S. & Flanagan, J. R. Coding and use of tactile signals from the fingertips in object manipulation tasks. *Nat. Rev. Neurosci.* **10**, 345–359 (2009).
5. Ingram, J. N. & Wolpert, D. M. Naturalistic approaches to sensorimotor control. *Prog. Brain Res.* **191**, 3–29 (2011).
6. Westling, G. & Johansson, R. S. Factors influencing the force control during precision grip. *Exp. Brain Res.* **53**, 277–284 (1984).
7. Johansson, R. S. & Westling, G. Coordinated isometric muscle commands adequately and erroneously programmed for the weight during lifting task with precision grip. *Exp. Brain Res.* **71**, 59–71 (1988).
8. Gordon, A. M., Westling, G., Cole, K. J. & Johansson, R. S. Memory representations underlying motor commands used during manipulation of common and novel objects. *J. Neurophysiol.* **69**, 1789–1796 (1993).
9. Flanagan, J. R. & Beltzner, M. A. Independence of perceptual and sensorimotor predictions in the size–weight illusion. *Nat. Neurosci.* **3**, 737–741 (2000).
10. Baugh, L. A., Kao, M., Johansson, R. S. & Flanagan, J. R. Material evidence: interaction of well-learned priors and sensorimotor memory when lifting objects. *J. Neurophysiol.* **108**, 1262–1269 (2012).
11. Flanagan, J. R., Bowman, M. C. & Johansson, R. S. Control strategies in object manipulation tasks. *Curr. Opin. Neurobiol.* **16**, 650–659 (2006).
12. Fu, Q. & Santello, M. Context-dependent learning interferes with visuomotor transformations for manipulation planning. *J. Neurosci.* **32**, 15086–15092 (2012).
13. Fu, Q. & Santello, M. Retention and interference of learned dexterous manipulation: interaction between multiple sensorimotor processes. *J. Neurophysiol.* **113**, 144–155 (2015).
14. Wolpert, D. M. & Flanagan, J. R. Q&A: robotics as a tool to understand the brain. *BMC Biol.* **8**, 92 (2010).
15. Shadmehr, R. & Mussa-Ivaldi, F. A. Adaptive representation of dynamics during learning of a motor task. *J. Neurosci.* **14**, 3208–3224 (1994).
16. Dingwell, J. B., Mah, C. D. & Mussa-Ivaldi, F. A. Manipulating objects with internal degrees of freedom: evidence for model-based control. *J. Neurophysiol.* **88**, 222–235 (2002).
17. Dingwell, J. B., Mah, C. D. & Mussa-Ivaldi, F. A. Experimentally confirmed mathematical model for human control of a non-rigid object. *J. Neurophysiol.* **91**, 1158–1170 (2004).
18. Nagengast, A. J., Braun, D. A. & Wolpert, D. M. Optimal control predicts human performance on objects with internal degrees of freedom. *PLoS Comput. Biol.* **5**, e1000419 (2009).
19. Nasseroleslami, B., Hasson, C. J. & Sternad, D. Rhythmic manipulation of objects with complex dynamics: predictability over chaos. *PLoS Comput. Biol.* **10**, e1003900 (2014).
20. Flanagan, J. R. & Wing, A. M. The role of internal models in motion planning and control: evidence from grip force adjustments during movements of hand-held loads. *J. Neurosci.* **17**, 1519–1528 (1997).
21. Ahmed, A. A., Wolpert, D. M. & Flanagan, J. R. Flexible representations of dynamics are used in object manipulation. *Curr. Biol.* **18**, 763–768 (2008).
22. Danion, F., Diamond, J. S. & Flanagan, J. R. The role of haptic feedback when manipulating nonrigid objects. *J. Neurophysiol.* **107**, 433–441 (2012).
23. Sheahan, H. R., Franklin, D. W. & Wolpert, D. M. Motor planning, not execution, separates motor memories. *Neuron* **92**, 773–779 (2016).
24. Smith, M. A., Ghazizadeh, A. & Shadmehr, R. Interacting adaptive processes with different timescales underlie short-term motor learning. *PLoS Biol.* **4**, e179 (2006).
25. Scheidt, R. A., Reinkensmeyer, D. J., Colborn, M. A., Rymer, W. Z. & Mussa-Ivaldi, F. A. Persistence of motor adaptation during constrained, multi-joint, arm movements. *J. Neurophysiol.* **84**, 853–862 (2000).

26. Cothros, N., Wong, J. D. & Gribble, P. L. Are there distinct neural representations of object and limb dynamics? *Exp. Brain Res.* **173**, 689–697 (2006).
27. Kluzik, J., Diedrichsen, J., Shadmehr, R. & Bastian, A. J. Reach adaptation: what determines whether we learn an internal model of the tool or adapt the model of our arm? *J. Neurophysiol.* **100**, 1455–1464 (2008).
28. Gandolfo, F., Mussa-Ivaldi, F. A. & Bizzi, E. Motor learning by field approximation. *Proc. Natl Acad. Sci. USA* **93**, 3843–3846 (1996).
29. Howard, I. S., Wolpert, D. M. & Franklin, D. W. The effect of contextual cues on the encoding of motor memories. *J. Neurophysiol.* **109**, 2632–2644 (2013).
30. Salimi, I., Hollender, I., Frazier, W. & Gordon, A. M. Specificity of internal representations underlying grasping. *J. Neurophysiol.* **84**, 2390–2397 (2000).
31. Bursztyn, L. L. & Flanagan, J. R. Sensorimotor memory of weight asymmetry in object manipulation. *Exp. Brain Res.* **184**, 127–133 (2008).
32. Ingram, J. N., Howard, I. S., Flanagan, J. R. & Wolpert, D. M. Multiple grasp-specific representations of tool dynamics mediate skillful manipulation. *Curr. Biol.* **20**, 618–623 (2010).
33. Ingram, J. N., Howard, I. S., Flanagan, J. R. & Wolpert, D. M. A single-rate context-dependent learning process underlies rapid adaptation to familiar object dynamics. *PLoS Comput. Biol.* **7**, e1002196 (2011).
34. Ingram, J. N., Flanagan, J. R. & Wolpert, D. M. Context-dependent decay of motor memories during skill acquisition. *Curr. Biol.* **23**, 1107–1112 (2013).
35. Milner, T. E. & Franklin, D. W. Impedance control and internal model use during the initial stage of adaptation to novel dynamics in humans. *J. Physiol.* **567**, 651–664 (2005).
36. Howard, I. S., Ingram, J. N., Franklin, D. W. & Wolpert, D. M. Gone in 0.6 seconds: the encoding of motor memories depends on recent sensorimotor states. *J. Neurosci.* **32**, 12756–12768 (2012).
37. Berniker, M., Franklin, D. W., Flanagan, J. R., Wolpert, D. M. & Kording, K. Motor learning of novel dynamics is not represented in a single global coordinate system: evaluation of mixed coordinate representations and local learning. *J. Neurophysiol.* **111**, 1165–1182 (2014).
38. Nozaki, D. & Scott, S. H. Multi-compartment model can explain partial transfer of learning within the same limb between unimanual and bimanual reaching. *Exp. Brain Res.* **194**, 451–463 (2009).
39. Lee, J. Y. & Schweighofer, N. Dual adaptation supports a parallel architecture of motor memory. *J. Neurosci.* **29**, 10396–10404 (2009).
40. Kim, S., Oh, Y. & Schweighofer, N. Between-trial forgetting due to interference and time in motor adaptation. *PLoS ONE* **10**, e0142963 (2015).
41. Thoroughman, K. A. & Shadmehr, R. Learning of action through adaptive combination of motor primitives. *Nature* **407**, 742–747 (2000).
42. Trewartha, K. M., Garcia, A., Wolpert, D. M. & Flanagan, J. R. Fast but fleeting: adaptive motor learning processes associated with aging and cognitive decline. *J. Neurosci.* **34**, 13411–13421 (2014).
43. Ackerson, G. & Fu, K. On state estimation in switching environments. *IEEE Trans. Autom. Contr.* **15**, 10–17 (1970).
44. Chang, C. B. & Athans, M. State estimation for discrete systems with switching parameters. *IEEE Trans. Aerosp. Electron. Syst.* **14**, 418–425 (1978).
45. Shumway, R. H. & Stoffer, D. S. Dynamic linear models with switching. *J. Am. Stat. Assoc.* **86**, 763–769 (1991).
46. Howard, I. S., Wolpert, D. M. & Franklin, D. W. The value of the follow-through derives from motor learning depending on future actions. *Curr. Biol.* **25**, 397–401 (2015).
47. Nozaki, D., Kurtzer, I. & Scott, S. H. Limited transfer of learning between unimanual and bimanual skills within the same limb. *Nat. Neurosci.* **9**, 1364–1366 (2006).
48. Yokoi, A., Hirashima, M. & Nozaki, D. Gain field encoding of the kinematics of both arms in the internal model enables flexible bimanual action. *J. Neurosci.* **31**, 17058–17068 (2011).
49. Richter, S., Jansen-Osmann, P., Konczak, J. & Kalveram, K.-T. Motor adaptation to different dynamic environments is facilitated by indicative context stimuli. *Psychol. Res.* **68**, 245–251 (2004).
50. Yeo, S.-H., Wolpert, D. M. & Franklin, D. W. Coordinate representations for interference reduction in motor learning. *PLoS ONE* **10**, e0129388 (2015).
51. Hwang, E. J., Smith, M. A. & Shadmehr, R. Dissociable effects of the implicit and explicit memory systems on learning control of reaching. *Exp. Brain Res.* **173**, 425–437 (2006).
52. Hirashima, M. & Nozaki, D. Distinct motor plans form and retrieve distinct motor memories for physically identical movements. *Curr. Biol.* **22**, 432–436 (2012).
53. Chib, V. S., Krutky, M. A., Lynch, K. M. & Mussa-Ivaldi, F. A. The separate neural control of hand movements and contact forces. *J. Neurosci.* **29**, 3939–3947 (2009).
54. Casadio, M., Pressman, A. & Mussa-Ivaldi, F. A. Learning to push and learning to move: the adaptive control of contact forces. *Front. Comput. Neurosci.* **9**, 118 (2015).
55. Iriki, A., Tanaka, M. & Iwamura, Y. Coding of modified body schema during tool use by macaque postcentral neurones. *Neuroreport* **7**, 2325–2330 (1996).
56. Yamamoto, S. & Kitazawa, S. Sensation at the tips of invisible tools. *Nat. Neurosci.* **4**, 979–980 (2001).
57. Farnè, A., Iriki, A. & Làdavas, E. Shaping multisensory action–space with tools: evidence from patients with cross-modal extinction. *Neuropsychologia* **43**, 238–248 (2005).
58. Witt, J. K., Proffitt, D. R. & Epstein, W. Tool use affects perceived distance, but only when you intend to use it. *J. Exp. Psychol. Hum. Percept. Perform.* **31**, 880–888 (2005).
59. Haggard, P. W. & Wolpert, D. M. in *Higher-Order Motor Disorders* Ch. 14 (Oxford Univ. Press, Oxford, 2004).
60. Benton, A. L. *Right–Left Discrimination and Finger Localization: Development and Pathology* (Hoeber-Harper, New York, NY, 1959).
61. Jacobs, R. A., Jordan, M. I., Nowlan, S. J. & Hinton, G. E. Adaptive mixtures of local experts. *Neural Comput.* **3**, 79–87 (1991).
62. Wolpert, D. M. & Kawato, M. Multiple paired forward and inverse models for motor control. *Neural Netw.* **11**, 1317–1329 (1998).
63. Ghahramani, Z. & Hinton, G. E. Variational learning for switching state-space models. *Neural Comput.* **12**, 831–864 (2000).
64. Baddeley, R. J., Ingram, H. A. & Miall, R. C. System identification applied to a visuomotor task: near-optimal human performance in a noisy changing task. *J. Neurosci.* **23**, 3066–3075 (2003).
65. Burge, J., Ernst, M. O. & Banks, M. S. The statistical determinants of adaptation rate in human reaching. *J. Vis.* **8**, 20.1–20.19 (2008).
66. Zarahn, E., Weston, G. D., Liang, J., Mazzoni, P. & Krakauer, J. W. Explaining savings for visuomotor adaptation: linear time-invariant state-space models are not sufficient. *J. Neurophysiol.* **100**, 2537–2548 (2008).
67. Huang, V. S. & Shadmehr, R. Persistence of motor memories reflects statistics of the learning event. *J. Neurophysiol.* **102**, 931–940 (2009).
68. Fox, E., Sudderth, E. B., Jordan, M. I. & Willsky, A. S. in *Advances in Neural Information Processing Systems 21* (eds Koller, D., Schuurmans, D., Bengio, Y. & Bottou, L.) 457–464 (Curran Associates, Red Hook, NY, 2009).
69. Oldfield, R. C. The assessment and analysis of handedness: the Edinburgh inventory. *Neuropsychologia* **9**, 97–113 (1971).
70. Howard, I. S., Ingram, J. N. & Wolpert, D. M. A modular planar robotic manipulandum with end-point torque control. *J. Neurosci. Methods* **181**, 199–211 (2009).
71. Ingram, J. N., Sadeghi, M., Flanagan, J. R. & Wolpert, D. M. An error-tuned model for sensorimotor learning. *PLoS Comput. Biol.* **13**, e1005883 (2017).
72. Land, M. F. & Furneaux, S. The knowledge base of the oculomotor system. *Philos. Trans. R. Soc. Lond. B Biol. Sci.* **352**, 1231–1239 (1997).
73. Johansson, R. S., Westling, G., Backstrom, A. & Flanagan, J. R. Eye–hand coordination in object manipulation. *J. Neurosci.* **21**, 6917–6932 (2001).
74. Land, M. F., Mennie, N. & Rusted, J. Eye movements and the roles of vision in activities of daily living: making a cup of tea. *Perception* **28**, 1311–1328 (1999).
75. Doucet, A., Gordon, N. J. & Kroshnamurthy, V. Particle filters for state estimation of jump Markov linear systems. *IEEE Trans. Signal Process.* **49**, 613–624 (2001).
76. Bar-Shalom, Y., Rong Li, X. & Kirubarajan, T. *Estimation with Applications to Tracking and Navigation* (John Wiley & Sons, New York, NY, 2001).
77. Dempster, A. P., Laird, N. M. & Rubin, D. B. Maximum likelihood from incomplete data via the EM algorithm. *J. R. Stat. Soc. Ser. B Stat. Methodol.* **39**, 1–38 (1977).
78. Cappé, O. & Moulines E. On-line expectation-maximization algorithm for latent data models. *J. R. Stat. Soc.* **71**, 593–613 (2009).
79. Cappé, O. Online EM algorithm for hidden Markov models. *J. Comput. Graph. Stat.* **20**, 728–749 (2011).
80. George, A. P. & Powell, W. B. Adaptive stepsizes for recursive estimation with applications in approximate dynamic programming. *Mach. Learn.* **65**, 167–198 (2006).
81. Robbins, H. & Monro, S. A stochastic approximation method. *Ann. Math. Stat.* **22**, 400–407 (1951).
82. Del Moral, P., Doucet, A. & Singh, S. Forward smoothing using sequential Monte Carlo. Preprint at https://arxiv.org/abs/1012.5390 (2010).
83. Özkan, E., Lindsten, F., Fritsche, C. & Gustafsson, F. Recursive maximum likelihood identification of jump Markov nonlinear systems. *IEEE Trans. Signal Process.* **63**, 754–765 (2015).
84. Kalman, R. E. A new approach to linear filtering and prediction problems. *J. Basic Eng.* **82**, 35–45 (1960).
85. Kass, R. E. & Raftery, A. E. Bayes factors. *J. Am. Stat. Assoc.* **90**, 773–795 (1995).
86. Jeffreys, H. *The Theory of Probability* (Oxford Univ. Press, Oxford, 1998).

Acknowledgements

We thank G. Žalalytė and A. Pantelides for assistance with the experiments, and S. Singh for advice on the model. We thank the Wellcome Trust, Royal Society (Noreen Murray Professorship in Neurobiology to D.M.W.), Engineering and Physical Sciences Research Council and Canadian Institutes of Health Research for support. The funders had no role in the study design, data collection and analysis, decision to publish or preparation of the manuscript.

Author contributions

All authors conceived and designed the experiments. J.B.H. performed the experiments, and developed and fit the SSSM. All authors wrote the paper, discussed the results and edited the manuscript.

Competing interests

The authors declare no competing interests.

Additional information

Supplementary information is available for this paper at https://doi.org/10.1038/s41562-018-0324-5.

Correspondence and requests for materials should be addressed to J.B.H.

nature research

Corresponding author(s): Daniel Wolpert

☐ Initial submission ☐ Revised version ☒ Final submission

Life Sciences Reporting Summary

Nature Research wishes to improve the reproducibility of the work that we publish. This form is intended for publication with all accepted life science papers and provides structure for consistency and transparency in reporting. Every life science submission will use this form; some list items might not apply to an individual manuscript, but all fields must be completed for clarity.

For further information on the points included in this form, see Reporting Life Sciences Research. For further information on Nature Research policies, including our data availability policy, see Authors & Referees and the Editorial Policy Checklist.

Experimental design

1. Sample size

Describe how sample size was determined.

To provide sufficient power, sample sizes were chosen on the basis of the typical between-subject variability observed in similar motor adaptation studies.

2. Data exclusions

Describe any data exclusions.

Only pilot data (which was all run on lab members) was excluded from the published results.

3. Replication

Describe whether the experimental findings were reliably reproduced.

Our main finding that opposing dynamics can be learned when controlling different points on an object was replicated in three of the presented experiments.

4. Randomization

Describe how samples/organisms/participants were allocated into experimental groups.

Participant allocation was randomized prior to data collection.

5. Blinding

Describe whether the investigators were blinded to group allocation during data collection and/or analysis.

The investigators were not blinded to group allocation during data collection and/or analysis. Analysis is fully objective requiring no experimenter input

Note: all studies involving animals and/or human research participants must disclose whether blinding and randomization were used.

6. Statistical parameters

For all figures and tables that use statistical methods, confirm that the following items are present in relevant figure legends (or in the Methods section if additional space is needed).

n/a	Confirmed
☐	☒ The exact sample size (*n*) for each experimental group/condition, given as a discrete number and unit of measurement (animals, litters, cultures, etc.)
☐	☒ A description of how samples were collected, noting whether measurements were taken from distinct samples or whether the same sample was measured repeatedly
☒	☐ A statement indicating how many times each experiment was replicated
☐	☒ The statistical test(s) used and whether they are one- or two-sided (note: only common tests should be described solely by name; more complex techniques should be described in the Methods section)
☐	☒ A description of any assumptions or corrections, such as an adjustment for multiple comparisons
☐	☒ The test results (e.g. *P* values) given as exact values whenever possible and with confidence intervals noted
☐	☒ A clear description of statistics including central tendency (e.g. median, mean) and variation (e.g. standard deviation, interquartile range)
☐	☒ Clearly defined error bars

See the web collection on statistics for biologists for further resources and guidance.

Software

Policy information about availability of computer code

7. Software

Describe the software used to analyze the data in this study.	Data were analyzed in Matlab 2017a.

For manuscripts utilizing custom algorithms or software that are central to the paper but not yet described in the published literature, software must be made available to editors and reviewers upon request. We strongly encourage code deposition in a community repository (e.g. GitHub). *Nature Methods* guidance for providing algorithms and software for publication provides further information on this topic.

Materials and reagents

Policy information about availability of materials

8. Materials availability

Indicate whether there are restrictions on availability of unique materials or if these materials are only available for distribution by a for-profit company.	No unique materials were used in the study.

9. Antibodies

Describe the antibodies used and how they were validated for use in the system under study (i.e. assay and species).	n/a

10. Eukaryotic cell lines

a. State the source of each eukaryotic cell line used.	n/a
b. Describe the method of cell line authentication used.	n/a
c. Report whether the cell lines were tested for mycoplasma contamination.	n/a
d. If any of the cell lines used are listed in the database of commonly misidentified cell lines maintained by ICLAC, provide a scientific rationale for their use.	n/a

Animals and human research participants

Policy information about studies involving animals; when reporting animal research, follow the ARRIVE guidelines

11. Description of research animals

Provide details on animals and/or animal-derived materials used in the study.	No non-human animals were used in the study.

Policy information about studies involving human research participants

12. Description of human research participants

Describe the covariate-relevant population characteristics of the human research participants.	Fifty neurologically intact participants (22 males and 28 females; age 28.2 ± 7.8, mean ± SD) were recruited to participate in four experiments. All participants were right-handed according to the Edinburgh handedness inventory.

nature human behaviour

SUPPLEMENTARY INFORMATION

https://doi.org/10.1038/s41562-018-0324-5

In the format provided by the authors and unedited.

Multiple motor memories are learned to control different points on a tool

James B. Heald[1]*, James N. Ingram[1], J. Randall Flanagan[2] and Daniel M. Wolpert[1]

[1]Computational and Biological Learning Laboratory, Department of Engineering, University of Cambridge, Cambridge, UK. [2]Center for Neuroscience Studies and Department of Psychology, Queen's University, Kingston, ON, Canada. *e-mail: jbh40@cam.ac.uk

Multiple motor memories are learned to control different points on a tool

Supplementary Information

James B. Heald[1*], James N. Ingram[1], J. Randall Flanagan[2] & Daniel M. Wolpert[1]

[1] Computational and Biological Learning Lab, Department of Engineering,
University of Cambridge, Cambridge, CB2 1PZ, United Kingdom
[2] Center for Neuroscience Studies and Department of Psychology,
Queen's University, Kingston, ON, Canada

*Corresponding author: jbh40@cam.ac.uk

Supplementary Figures

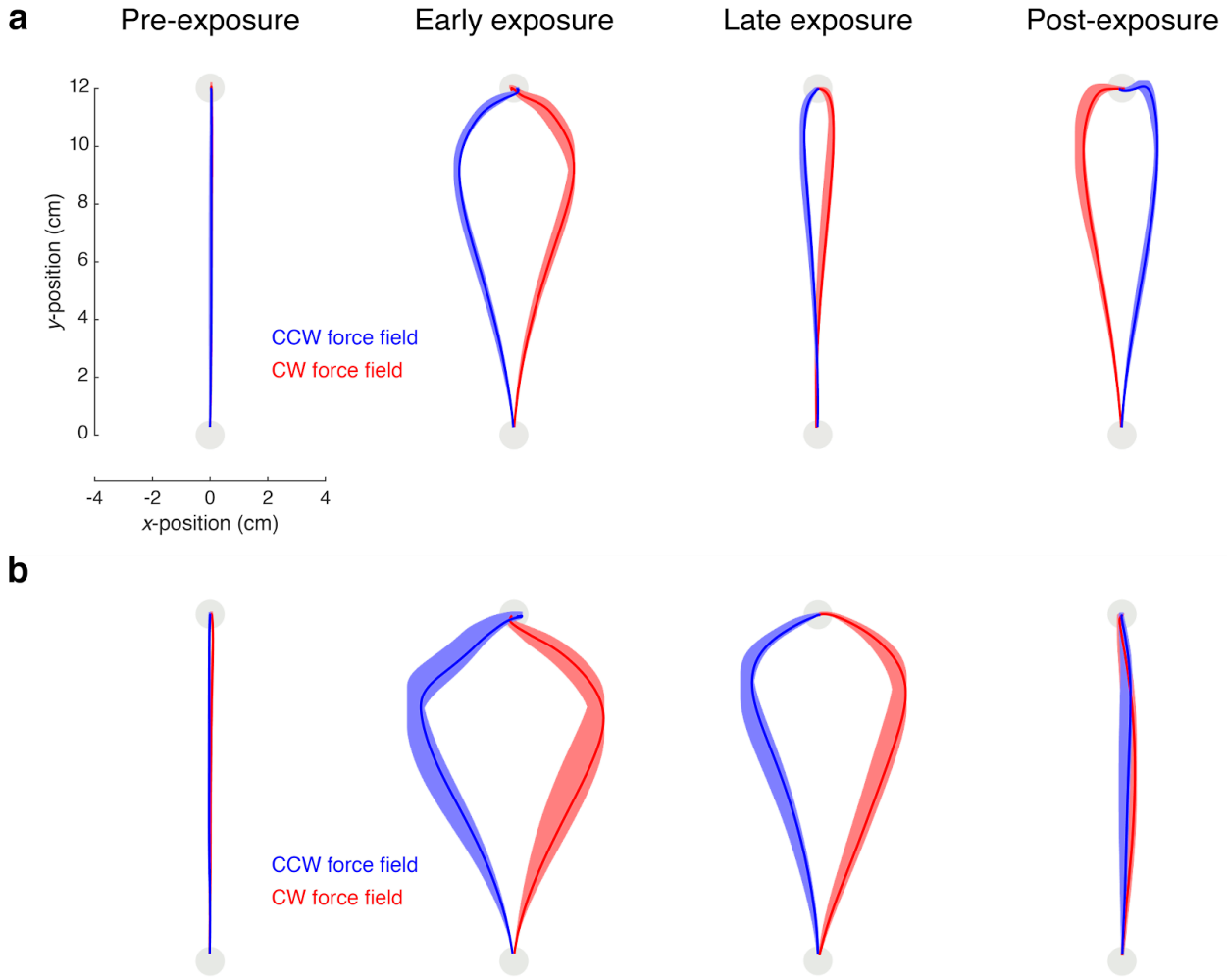

Supplementary Figure 1 | Hand paths at different stages of Experiment 1. a,b, In early exposure, the force fields produced substantial deviations of the hand path from a straight line. For the two-control-points groups (n = 10) **(a)**, hand paths were significantly straighter by late exposure, and clear after-effects were seen in early post-exposure. For the single-control-point group (n = 8) **(b)**, hand paths were not significantly straighter by late exposure, and no after-effects were seen. Traces show mean ± s.e.m. across participants hand paths over two blocks.

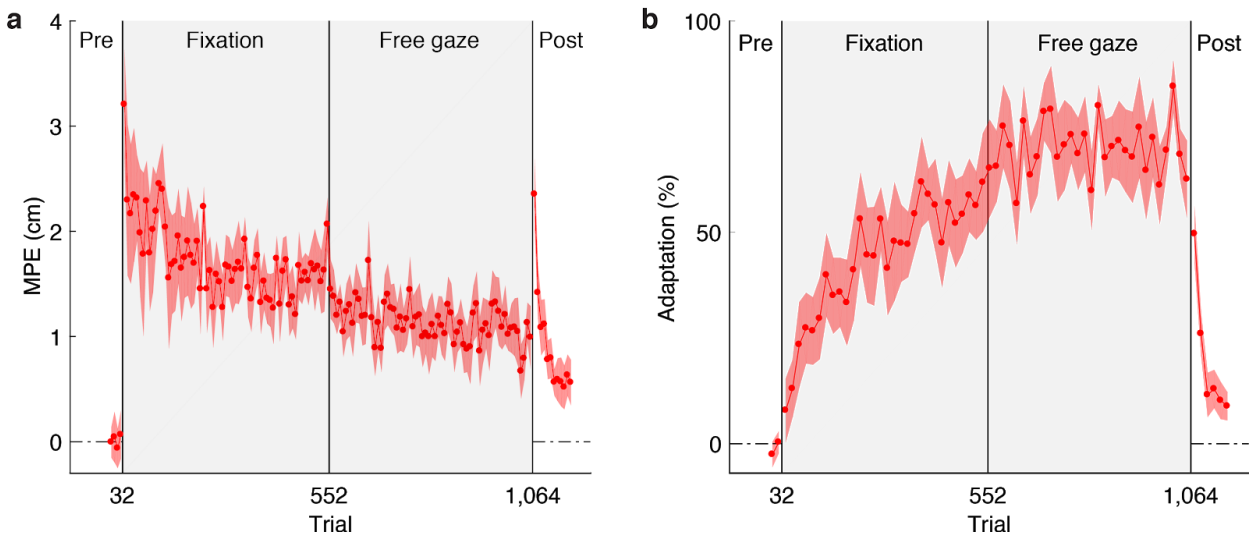

Supplementary Figure 2 | Adaptation is not gaze dependent. In the fixation stage of the exposure phase, participants (n = 8) were required to fixate a cross in the midline of the workspace. In the free-gaze stage of the exposure phase, no fixation cross was displayed and gaze was unconstrained. **a,b,** Mean ± s.e.m. **(a)** MPE and **(b)** adaptation across all participants. Each MPE data point represents the mean of a block of eight trials. To assess learning, we compared adaptation in the final two blocks of the pre-exposure phase with the final two blocks of the fixation stage. We found a significant increase in adaptation (two-tailed paired t-test, 60.2 ± 8.4%, t_7 = 7.70, P = 1 x 10^{-4}), which reached 59.0 ± 7.9% (mean ± s.e.m.) of full compensation by the final two blocks of the fixation stage. We contrasted the adaptation reached by blocks 23-24 of the exposure phase with the two-control-points and opposing-field groups who experienced the same task with free gaze. This revealed no significant difference (between-subjects ANOVA, $F_{2,23}$ = 2.07, P = 0.149), indicating that fixation did not detriment learning. We allowed the fixation group to continue exposure after the fixation phase but with free gaze. There was no significant additional learning after 616 further trials (two-tailed paired t-test, 6.4 ± 10.4%, t_7 = 0.67, P = 0.526).

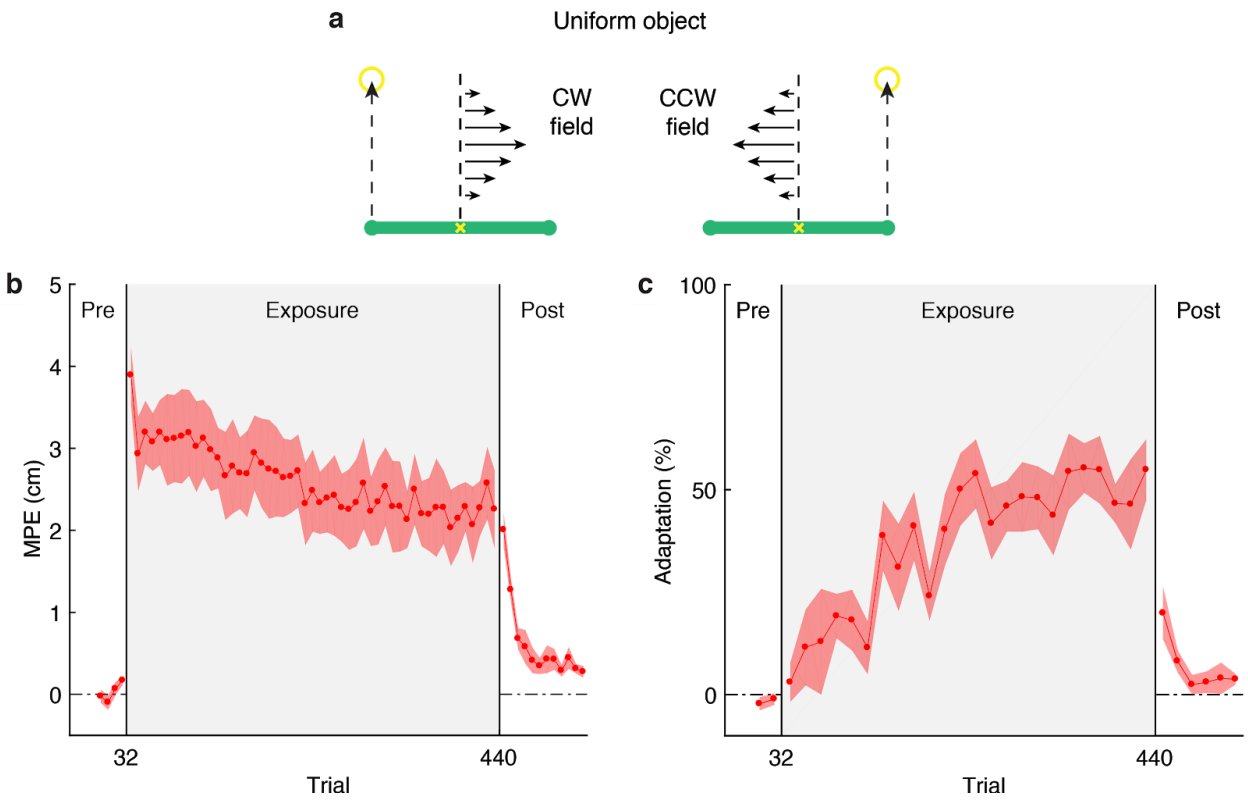

Supplementary Figure 3 | Adaptation does not require control points to be distinct from the rest of the object. **a,** Participants (n = 8) controlled a uniform object composed of two green disks connected by a green bar. Because the disks and bar were the same color, the object did not contain any distinct visual elements. **b,c,** Mean ± s.e.m. **(b)** MPE and **(c)** adaptation across all participants. Each MPE data point represents the mean of a block of eight trials. To assess learning, we compared adaptation in the final two blocks of the pre-exposure phase with the final two blocks of the exposure phase. We found a significant increase in adaptation (two-tailed paired t-test, 52.3 ± 9.3%, t_7 = 6.08, P = 5 x 10^{-4}), which reached 50.7 ± 8.5% (mean ± s.e.m.) of full compensation by the final two blocks of the exposure phase. We contrasted the adaptation reached by this stage with the two-control-point and opposing-field groups who experienced the same task with control points displayed as green disks on a red rectangle. There was no significant difference (between-subjects ANOVA, $F_{2,23}$ = 2.11, P = 0.144), indicating that the uniform object did not detriment learning.

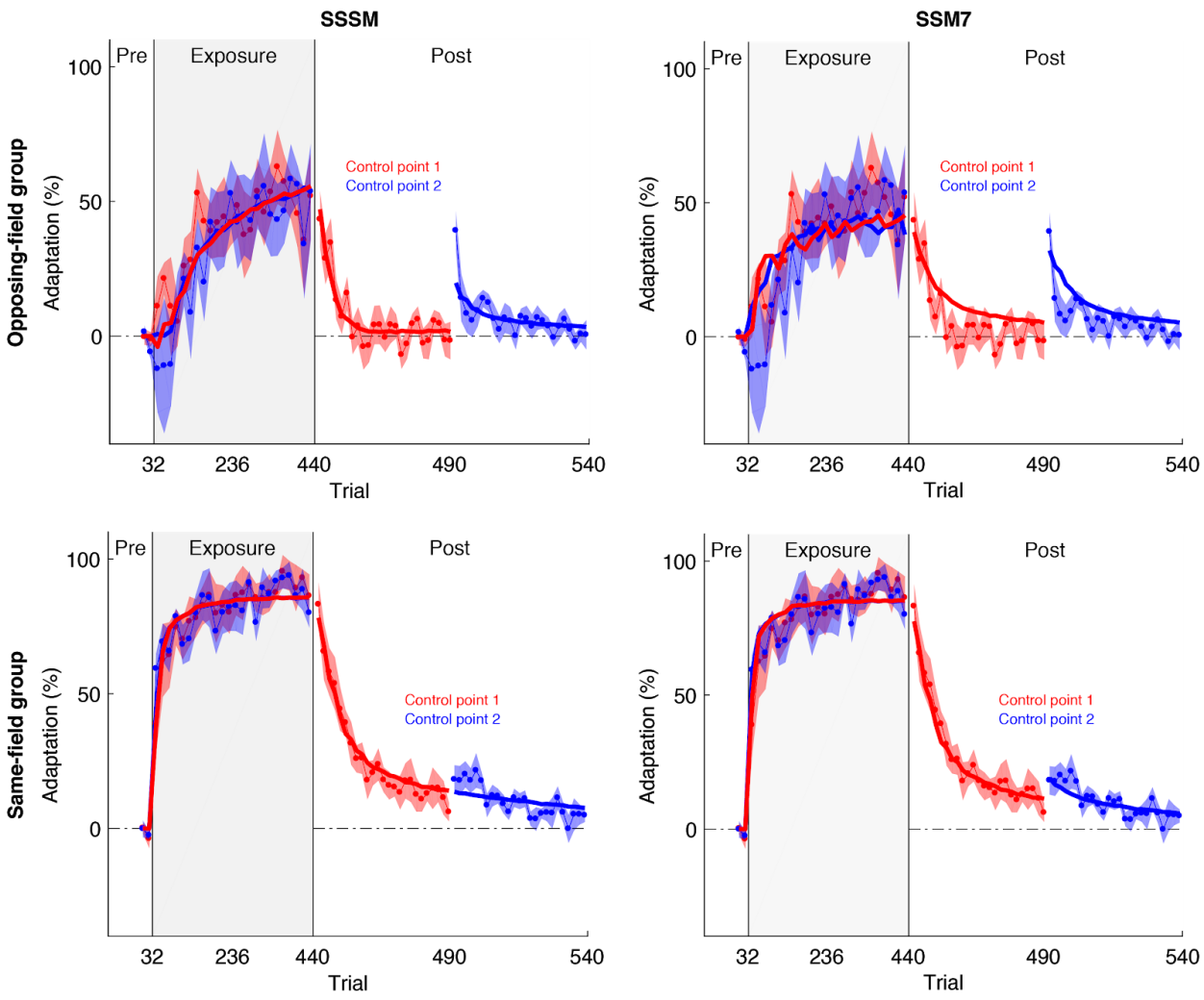

Supplementary Figure 4 | Model fits to adaptation data from Experiment 2. Solid lines show the mean fits across participants for the switching state-space model (SSSM) and state-space model 7 (SSM7), which had the next best BIC. Experimental data is shown as in Fig. 3b,d for the opposing-field (n = 8) and same-field (n = 8) groups. The superiority of the SSSM is most apparent in the fit to data from the opposing-field group.

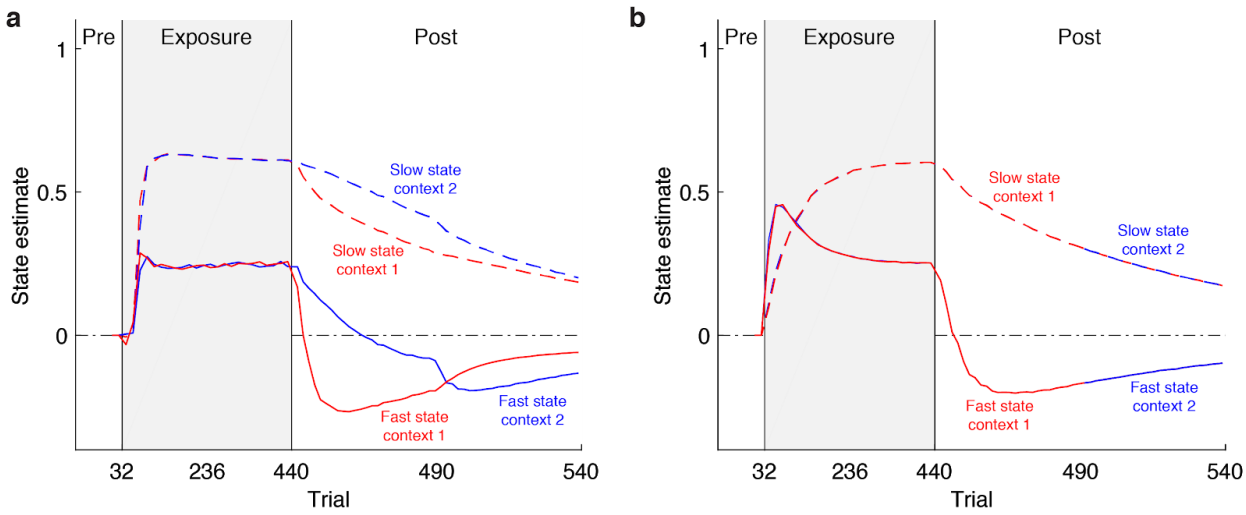

Supplementary Figure 5 | Slow and fast states of the switching state-space model. a, Mean state estimates across participants for the group that experienced opposing force fields at each control point. The slow and fast states of each context learn to represent different perturbations and, due to the learned association between contexts and cues, de-adapt at different rates during washout. For simplicity, the signs of the slow and fast states for context 2 have been inverted. **b,** For the group that experienced the same force field at each control point, the slow and fast states of each context represent the same perturbation and de-adapt at the same rate during washout.

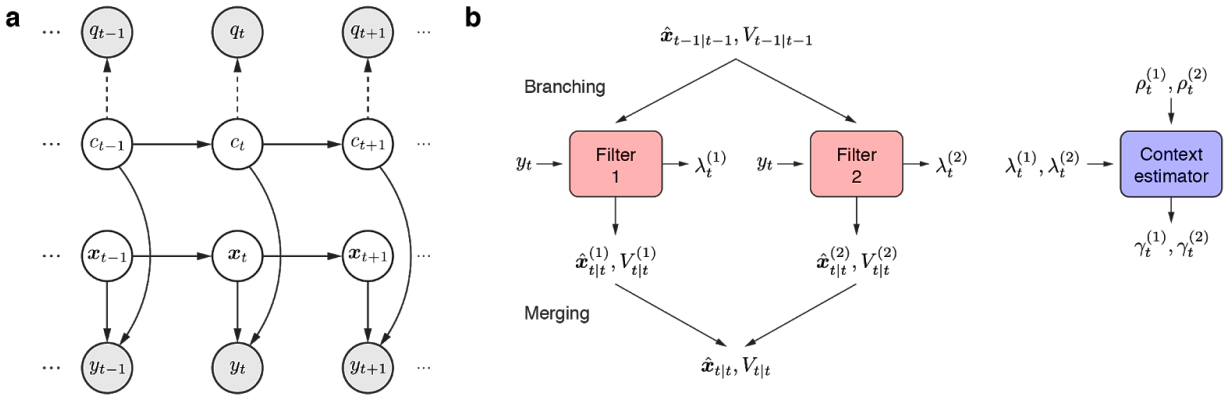

Supplementary Figure 6 | Motor adaptation as online state and parameter estimation in a switching state-space model. a, The graphical model. The discrete context, c_t, and the continuous perturbations, $\boldsymbol{x}_t$, evolve according to Markovian dynamics. The context determines both which observable cue, q_t, is emitted and how each perturbation contributes to the continuous observation y_t. Observed and latent variables are represented by gray and white nodes, respectively. The dashed arrows indicate dependencies that are learned online. **b,** The GPB1 algorithm. Given a single estimate of the state on trial $t-1$, each Kalman filter predicts the state on trial t and then updates its prediction when y_t is observed. The updated estimates of each filter are then merged into a single estimate. The probability of each context, which depends on both the contextual cue and the prediction error of each filter, determines how to merge the estimates in an optimal manner.

Supplementary Tables

Supplementary Table 1 | Variants of the context-dependent state-space model

Model	DOF	Retention vector ***a***	Learning-rate vector ***b***	Context vector ***c***	Number of effective states
SSM1[1]	3	$\begin{bmatrix} a_s & 0 & a_s & 0 \end{bmatrix}^{\mathrm{T}}$	$\begin{bmatrix} b_s & 0 & b_s & 0 \end{bmatrix}^{\mathrm{T}}$	$\boldsymbol{c}^{(1)} = \begin{bmatrix} 1 & 0 & c_s & 0 \end{bmatrix}^{\mathrm{T}}$ $\boldsymbol{c}^{(2)} = \begin{bmatrix} c_s & 0 & 1 & 0 \end{bmatrix}^{\mathrm{T}}$	2
SSM2[2]	3	$\begin{bmatrix} a & a & a & 0 \end{bmatrix}^{\mathrm{T}}$	$\begin{bmatrix} b_{\mathrm{s}} & b_{\mathrm{f}} & b_{\mathrm{s}} & 0 \end{bmatrix}^{\mathrm{T}}$	$\boldsymbol{c}^{(1)} = \begin{bmatrix} 1 & 1 & 0 & 0 \end{bmatrix}^{\mathrm{T}}$ $\boldsymbol{c}^{(2)} = \begin{bmatrix} 0 & 1 & 1 & 0 \end{bmatrix}^{\mathrm{T}}$	3
SSM3[1]	4	$\begin{bmatrix} a_{\mathrm{s}} & a_{\mathrm{f}} & a_{\mathrm{s}} & 0 \end{bmatrix}^{\mathrm{T}}$	$\begin{bmatrix} b_{\mathrm{s}} & b_{\mathrm{f}} & b_{\mathrm{s}} & 0 \end{bmatrix}^{\mathrm{T}}$	$\boldsymbol{c}^{(1)} = \begin{bmatrix} 1 & 1 & 0 & 0 \end{bmatrix}^{\mathrm{T}}$ $\boldsymbol{c}^{(2)} = \begin{bmatrix} 0 & 1 & 1 & 0 \end{bmatrix}^{\mathrm{T}}$	3
SSM4[1]	5	$\begin{bmatrix} a_{\mathrm{s}} & a_{\mathrm{f}} & a_{\mathrm{s}} & 0 \end{bmatrix}^{\mathrm{T}}$	$\begin{bmatrix} b_{\mathrm{s}} & b_{\mathrm{f}} & b_{\mathrm{s}} & 0 \end{bmatrix}^{\mathrm{T}}$	$\boldsymbol{c}^{(1)} = \begin{bmatrix} 1 & 1 & c_{\mathrm{s}} & 0 \end{bmatrix}^{\mathrm{T}}$ $\boldsymbol{c}^{(2)} = \begin{bmatrix} c_{\mathrm{s}} & 1 & 1 & 0 \end{bmatrix}^{\mathrm{T}}$	3
SSM5[1]	5	$\begin{bmatrix} a_{\mathrm{s}} & a_{\mathrm{f}} & a_{\mathrm{s}} & a_{\mathrm{f}} \end{bmatrix}^{\mathrm{T}}$	$\begin{bmatrix} b_{\mathrm{s}} & b_{\mathrm{f}} & b_{\mathrm{s}} & b_{\mathrm{f}} \end{bmatrix}^{\mathrm{T}}$	$\boldsymbol{c}^{(1)} = \begin{bmatrix} 1 & 1 & 0 & c_{\mathrm{f}} \end{bmatrix}^{\mathrm{T}}$ $\boldsymbol{c}^{(2)} = \begin{bmatrix} 0 & c_{\mathrm{f}} & 1 & 1 \end{bmatrix}^{\mathrm{T}}$	4
SSM6[1]	5	$\begin{bmatrix} a_{\mathrm{s}} & a_{\mathrm{f}} & a_{\mathrm{s}} & a_{\mathrm{f}} \end{bmatrix}^{\mathrm{T}}$	$\begin{bmatrix} b_{\mathrm{s}} & b_{\mathrm{f}} & b_{\mathrm{s}} & b_{\mathrm{f}} \end{bmatrix}^{\mathrm{T}}$	$\boldsymbol{c}^{(1)} = \begin{bmatrix} 1 & 1 & c_{\mathrm{s}} & 0 \end{bmatrix}^{\mathrm{T}}$ $\boldsymbol{c}^{(2)} = \begin{bmatrix} c_{\mathrm{s}} & 0 & 1 & 1 \end{bmatrix}^{\mathrm{T}}$	4
SSM7[1]	6	$\begin{bmatrix} a_{\mathrm{s}} & a_{\mathrm{f}} & a_{\mathrm{s}} & a_{\mathrm{f}} \end{bmatrix}^{\mathrm{T}}$	$\begin{bmatrix} b_{\mathrm{s}} & b_{\mathrm{f}} & b_{\mathrm{s}} & b_{\mathrm{f}} \end{bmatrix}^{\mathrm{T}}$	$\boldsymbol{c}^{(1)} = \begin{bmatrix} 1 & 1 & c_{\mathrm{s}} & c_{\mathrm{f}} \end{bmatrix}^{\mathrm{T}}$ $\boldsymbol{c}^{(2)} = \begin{bmatrix} c_{\mathrm{s}} & c_{\mathrm{f}} & 1 & 1 \end{bmatrix}^{\mathrm{T}}$	4

We examined 7 context-dependent state-space models, which varied in their number of parameters (DOF). The models could vary in the retention parameters, learning rates and coupling. The setting of the parameters determine the effective number of states in each model. Note that models 2-4 do not map the states on to contexts 1 and 2 in equation (4) as one of the states is shared by both contexts (i.e., context independent). Furthermore, model 2 does not necessarily map the states on to the fast and slow states in equation (4) as the context-independent state can be either fast or slow.

Supplementary Table 2 | Comparison of model fits for the state-space (SSM) and switching state-space (SSSM) models

State-space models	R^2	ΔBIC	DOF	a_s	b_s	c_s	a_f	b_f	c_f
SSM1	0.92	135.3	3	0.9858	0.0730	0.4578	-	-	-
SSM2	0.92	135.3	3	0.9858	0.0215	[0]	0.9858	0.0668	[1]
SSM3	0.92	140.6	4	0.9858	0.0215	[0]	0.9858	0.0668	[1]
SSM4	0.93	117.3	5	0.9905	0.0445	0.4040	0.9229	0.0922	[1]
SSM5	0.92	145.9	5	0.9862	0.0007	[0]	0.9858	0.0721	0.4636
SSM6	0.93	129.6	5	0.9895	0.0502	0.5234	0.8860	0.0553	[0]
SSM7	0.94	112.4	6	0.9932	0.0295	0.4660	0.9405	0.0888	0.4340

Switching state-space model				a_s	q_s	a_f	q_f	r	α
SSSM	0.96	0	6	0.9946	0.0003	0.9404	0.0068	0.0792	0.6067

Numbers in square brackets are fixed and not fit to the data. Note that although the R^2 values are similar these are independent of the number of data points, whereas the BIC scales with the number of data points. Therefore, the small improvement in R^2 for a model can translate into a large difference in likelihood and hence BIC. In SSM2, the fast state corresponds to the context-independent state shared by both contexts (see Supplementary Table 1 for details).

Supplementary References

1. Kim, S., Oh, Y. & Schweighofer, N. PLoS One 10, e0142963 (2015).
2. Nozaki, D. & Scott, S.H. Exp. Brain Res. 194, 451–463 (2009).